

Controlling chaos in a fast diode resonator using extended time-delay autosynchronization: Experimental observations and theoretical analysis

David W. Sukow, Michael E. Bleich, Daniel J. Gauthier, and Joshua E. S. Socolar
Department of Physics and Center for Nonlinear and Complex Systems, Duke University, P.O. Box 90305, Durham, North Carolina 27708

(Received 24 March 1997; accepted for publication 21 May 1997)

We stabilize unstable periodic orbits of a fast diode resonator driven at 10.1 MHz (corresponding to a drive period under 100 ns) using extended time-delay autosynchronization. Stabilization is achieved by feedback of an error signal that is proportional to the difference between the value of a state variable and an infinite series of values of the state variable delayed in time by integral multiples of the period of the orbit. The technique is easy to implement electronically and it has an all-optical counterpart that may be useful for stabilizing the dynamics of fast chaotic lasers. We show that increasing the weights given to temporally distant states enlarges the domain of control and reduces the sensitivity of the domain of control on the propagation delays in the feedback loop. We determine the average time to obtain control as a function of the feedback gain and identify the mechanisms that destabilize the system at the boundaries of the domain of control. A theoretical stability analysis of a model of the diode resonator in the presence of time-delay feedback is in good agreement with the experimental results for the size and shape of the domain of control. © 1997 American Institute of Physics. [S1054-1500(97)00104-3]

In this article we investigate a control scheme that is effective in suppressing deterministic chaos in fast dynamical systems. It is desirable to devise such schemes because the presence of deterministic chaos in devices generally degrades their performance in many applications. The signatures of chaos include erratic, noise-like fluctuations in the temporal evolution of the system variables, broadband features in the power spectrum, and the long-term behavior of the system is extreme sensitivity to applications of small perturbations to the system variables. Recent research has demonstrated that feedback control algorithms that take advantage of the special properties of chaotic systems are effective in controlling chaos. We review several specific control schemes and present our study of a continuous feedback scheme that is particularly well-suited for controlling chaotic systems that fluctuate on fast time scales. We present experimental results of the control of a fast chaotic electronic circuit and find good agreement with theoretical predictions.

I. INTRODUCTION

In many cases of practical importance, instabilities and chaos can seriously limit the performance of nonlinear dynamical systems. Obvious strategies for obtaining stable behavior are to redesign the entire system or integrate several sub-systems that cover the entire range of operating conditions, but these options may not be possible or appropriate for the application due to cost or space considerations, for example. An alternate method for obtaining stable behavior is to use control techniques that suppress the instabilities. Recently, researchers in the nonlinear dynamics community have demonstrated that such control can be achieved by making only small adjustments to some accessible system

parameter. The strength and timing of the adjustments can often be determined from algorithms that do not require detailed models of the dynamics.

The key idea underlying the new class of control schemes is to take advantage of the presence of unstable steady states (USSs) and unstable periodic orbits (UPOs) of the system (infinite in number).^{1,2} Figure 1 shows an example of chaotic oscillations in which the presence of UPOs is clearly evident with the appearance of nearly periodic oscillations during short intervals. (This figure illustrates the dynamical evolution of current flowing through an electronic diode resonator circuit studied in detail below.) The control protocols attempt to stabilize one such UPO³ by making small adjustments to an accessible parameter when the system is in a neighborhood of the state.⁴

Several research groups have demonstrated control of unstable states in a variety of physical, chemical, and biological systems.² In most cases, as detailed in other articles in this volume, the control protocol involves feedback based on the difference between the present state of the system and some externally generated reference signal representing the dynamics of the ideal unstable state. We focus instead on systems for which such a comparison is impractical, due to the speed of the oscillations or other difficulties in constructing the correct reference state. One example of a high-frequency system in which matching to an external reference is difficult is the diode resonator circuit studied in this paper. A second example of significant technological importance that clearly falls into this category are the semiconductor lasers used in state-of-the-art optical devices.⁵⁻⁷

We recently reported a new technique for stabilizing UPOs in low-dimensional dynamical systems that allows for control over a large domain of parameters and is well suited

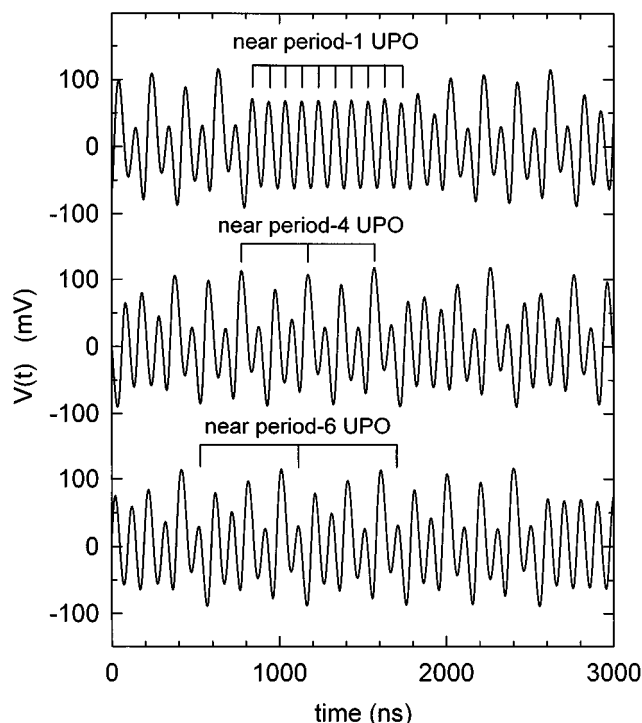


FIG. 1. Temporal evolution of a chaotic electronic circuit. The vertical axis $V(t)$ measures the voltage drop across a 50Ω resistor and is proportional to the current in the circuit. The system ergodically visits the unstable periodic orbits embedded with the chaotic attractor, three of which are indicated.

for practical implementation in fast systems.⁸ We refer to this scheme as ‘extended time-delay auto-synchronization’ (ETDAS): It uses a continuous feedback loop that attempts to synchronize the system with its own past behavior rather than an external reference. It is based on a scheme first published by Pyragas⁹ that involves the comparison of the present value of a state variable with its value one period of the UPO in the past, but extends that approach to include information from further in the past in a way that is easy to implement either electronically or optically. The efficacy of ETDAS was demonstrated by stabilizing the dynamics of a chaotic diode resonator driven at 10 MHz (a drive period of 100 ns).⁸ Since our report, Bleich and Socolar have developed a general mathematical technique for determining the stability of a nonlinear dynamical system in the presence of ETDAS feedback.¹⁰

In this paper we present a detailed account of the experimental work discussed in our previous report and compare the experimental results with a theoretical analysis of a model of the controlled diode resonator. In the next section, we review previously developed techniques for controlling chaos and highlight the issues that arise when attempting to control fast dynamical systems. In Sec. III, we describe ETDAS in detail and outline the general theoretical method for determining the stability of a dynamical system in the presence of time-delayed feedback. Section IV describes various implementations of ETDAS including an all-optical scheme for controlling the dynamics of fast optical systems and the specific electronic implementation for controlling the

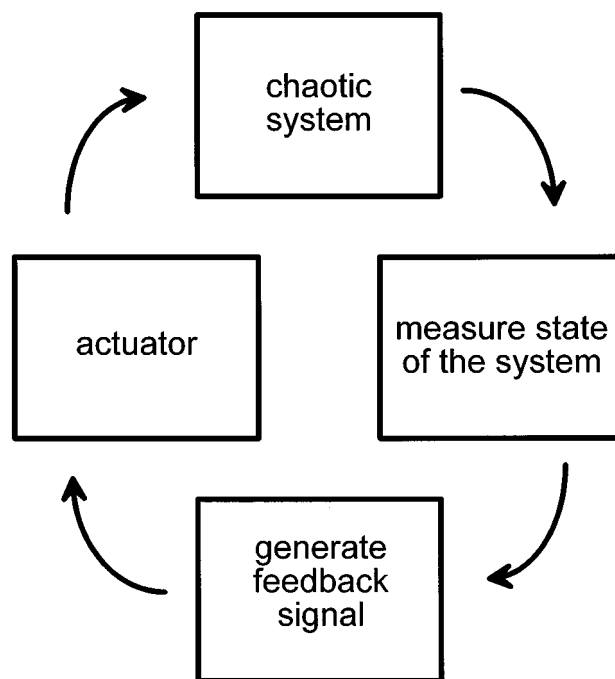


FIG. 2. Building blocks of a feedback scheme for controlling chaos.

diode resonator. Section V summarizes our experimental findings, and in Sec. VI we make concluding remarks and look to the future.

II. CONTROLLING CHAOS USING SMALL PERTURBATIONS

A. Brief historical review

Techniques for stabilizing unstable states in nonlinear dynamical systems using small perturbations fall into two general categories: Feedback and non-feedback schemes. In non-feedback (open-loop) schemes,^{11,12} an orbit similar to the desired unstable state is entrained by adjusting an accessible system parameter about its nominal value by a weak periodic signal, usually in the form of a continuous sinusoidal modulation. This is somewhat simpler than feedback schemes because it does not require real-time measurement of the state of the system and processing of a feedback signal. Unfortunately, period modulation fails in many cases to entrain the UPO (its success or failure is highly dependent on the specific form of the dynamical system¹³).

The possibility that chaos and instabilities can be controlled efficiently using feedback (closed loop) schemes to stabilize UPOs was suggested by Ott, Grebogi, and Yorke (OGY) in 1990.^{1,14} The basic building blocks of a generic feedback scheme consists of the chaotic system that is to be controlled, a device to sense the dynamical state of the system, a processor to generate the feedback signal, and an actuator that adjusts the accessible system parameter, as shown schematically in Fig. 2.

In their original conceptualization of the control scheme, OGY suggested the use of discrete proportional feedback

because of its simplicity and the fact that the control parameters can be determined straightforwardly from experimental observations. In this particular form of feedback control, the state of the system is sensed and adjustments are made to the accessible system parameter as the system passes through a surface of section. The size of the adjustments is proportional to the difference between the current and desired states of the system. Specifically, consider a system whose dynamics on a surface of section is governed by the m -dimensional map $\mathbf{z}_{i+1} = \mathbf{F}(\mathbf{z}_i, p_i)$, where \mathbf{z}_i is its location on the i th piercing of the surface and p_i is the value of an externally accessible control parameter that can be adjusted about a nominal value \bar{p} . Feedback control of the desired UPO (characterized by the location $\mathbf{z}_*(\bar{p})$ of its piercing through the section) is achieved by adjusting the accessible parameter by an amount $\delta p_i = p_i - \bar{p} = -\gamma \hat{\mathbf{n}} \cdot [\mathbf{z}_i - \mathbf{z}_*(\bar{p})]$ on each piercing of the section when \mathbf{z}_i is in a small neighborhood of $\mathbf{z}_*(\bar{p})$, where γ is the feedback gain and $\hat{\mathbf{n}}$ is a m -dimensional unit vector that is directed along the measurement direction.¹⁵ The location of the unstable fixed-point $\mathbf{z}_*(\bar{p})$ must be known before control is initiated; it can be determined from experimental observations of \mathbf{z}_i in the absence of control. The feedback gain γ and the measurement direction $\hat{\mathbf{n}}$ necessary to obtain control is determined from the local linear dynamics of the system about $\mathbf{z}_*(\bar{p})$ using the standard techniques of modern control engineering,^{1,16} and it is chosen so that the adjustments δp_i force the system onto the local stable manifold of the fixed point on the next piercing of the section. Successive iterates then collapse to $\mathbf{z}_*(\bar{p})$. It is important to note that δp_i vanishes when the system is stabilized; the control only has to counteract the destabilizing effects of noise.

Ditto *et al.*¹⁷ demonstrated the practicality of this technique by using it to control the dynamics of a chaotic magnetoelastic ribbon. They reconstructed the map using a time-delay embedding of a time series of a single variable and found that the discrete feedback control scheme is easy to implement, robust to noise, and rather insensitive to imprecise knowledge of $\mathbf{z}_*(\bar{p})$ and γ . Soon thereafter, Hunt¹⁸ and Peng, Petrov, and Showalter¹⁹ found that control can be obtained by occasionally delivering brief perturbations $\delta p_i = -\gamma[\zeta_i - \zeta_*(\bar{p})]\Theta(\tau_i)$ to the system parameter, where $\zeta_i = \hat{\mathbf{n}} \cdot \mathbf{z}_i$, and $\Theta(\tau_i)$ is a square pulse function of duration τ_i . Carr and Schwartz^{20,21} have considered delays and τ_i as control parameters. Often, γ , $\hat{\mathbf{n}}$, ζ_* , and τ_i are determined empirically by adjusting their values to obtain controlled behavior. Note again that δp_i vanishes when the UPO is controlled successfully. In the ensuing years, several discrete feedback control schemes that refine the original OGY concept have been devised and applied to experimental systems with natural frequencies ranging from 10^{-2} to 10^5 Hz.²

B. Controlling chaos in fast dynamical systems

Scaling these schemes to significantly higher frequencies, such as that encountered in high-speed electronic or optical systems, for example, is challenging for several rea-

sons. One important issue in high-speed feedback control of chaotic systems is the latency through the control loop, that is, the time t_ℓ between the sensing of the state of the system and the application of the control signal. The latency of the control loop is affected by the propagation speed of the signals through the components of the loop and the processing time of the feedback signal. An additional important issue is that it is difficult to accurately sample the state of the system at discrete times in order to compare it with the reference value and to rapidly adjust the control parameter on a time-scale comparable to the response time of the system.

Continuous feedback schemes avoid or reduce many of these problems and hence may be useful for controlling high-speed chaos. An obvious extension of the original OGY suggestion for controlling UPOs is to use continuous adjustment of the accessible system parameter by an amount $\delta p(t) = -\gamma \hat{\mathbf{n}} \cdot [\mathbf{x}(t) - \mathbf{x}_*(t)]$, where $\mathbf{x}(t)$ is the system trajectory, $\mathbf{x}_*(t)$ is the trajectory of the UPO in m -dimensional phase space, and γ is a constant feedback gain.^{9,22} This scheme is not amenable for controlling the dynamics of high-speed systems, however, because it is difficult to accurately determine, store, and regenerate $\mathbf{x}_*(t)$.

Several researchers have suggested that unstable steady states can be stabilized in high-speed systems using a class of continuous feedback techniques that do not require rapid switching or sampling, nor do they require a reference signal corresponding to the desired orbit. The USSs of a laser²³ and an electronic circuit²⁴ have been stabilized using continuous adjustment of the system parameter by an amount $\delta p(t) = -\gamma \hat{\mathbf{n}} \cdot [d\mathbf{x}(t)/dt]$, often called derivative control (these authors did not stress the high-speed capabilities of this control scheme). Note that $\delta p(t)$ vanishes when the system is stabilized to the USS and no explicit knowledge of the USS is required to implement control. The feedback gain γ is determined from the local linear dynamics of the system about the USS using the standard techniques of modern control engineering, or it can be determined empirically in experiments.

As first suggested by Pyragas,⁹ the UPOs of a dynamical system can be controlled using continuous feedback designed to synchronize the current state of the system and a time-delayed version of itself, with the time delay equal to one period of the desired orbit. Specifically, UPOs of period τ can be stabilized by continuous adjustment of the accessible parameter by an amount

$$\delta p(t) = -\gamma[\xi(t) - \xi(t - \tau)], \quad (1)$$

where γ is the feedback gain, $\xi(t) = \hat{\mathbf{n}} \cdot \mathbf{x}(t)$, and $\hat{\mathbf{n}}$ is the measurement direction. We refer to this method of control as 'time-delay autosynchronization' (TDAS). Note that $\delta p(t)$ vanishes when the system is on the UPO since $\xi(t) = \xi(t - \tau)$ for all t . This control scheme has been demonstrated experimentally in electronic circuits^{25,26} operating at frequencies of 10 MHz, and in lower frequency systems such as an electronic circuit,²⁷ a fiber laser,²⁸ a glow discharge,²⁹ a magneto-elastic ribbon,³⁰ and a periodically driven yttrium iron garnet film.³¹ In addition, TDAS has been demonstrated

theoretically to be effective for stabilizing the dynamics of a tunable semiconductor oscillator,³² neuronal networks,³³ lasers,^{34,35} and pattern forming systems.³⁶ The main drawback to TDAS is that it is not effective at controlling highly unstable orbits.²⁵

III. EXTENDED TIME-DELAY AUTOSYNCHRONIZATION

A. The ET DAS feedback scheme

Recently, three of us⁸ introduced a generalization of TDAS that is capable of extending the domain of effective control significantly³⁷ and is easy to implement in high-speed systems. Stabilization of UPOs of period τ is achieved by feedback of an error signal that is proportional to the difference between the value of a state variable and an infinite series of values of the state variable delayed in time by integral multiples of τ . Specifically, ET DAS prescribes the continuous adjustment of the system parameter by

$$\delta p(t) = -\gamma \left[\xi(t) - (1-R) \sum_{k=1}^{\infty} R^{k-1} \xi(t-k\tau) \right], \quad (2)$$

where $-1 \leq R < 1$ regulates the weight of information from the past.³⁸ As we will motivate in Sec. III C and see in Sec. V C, highly unstable orbits can be stabilized as $R \rightarrow 1$. The case $R=0$ corresponds to TDAS, the scheme introduced by Pyragas.⁹ We emphasize that, for any R , $\delta p(t)$ vanishes when the UPO is stabilized since $\xi(t-k\tau) = \xi(t)$ for all t and k , so there is no power dissipated in the feedback loop whenever ET DAS is successful. Note that no property of the UPO must be known in advance except its period. In periodically driven systems, where the period of the orbit is determined from the driving, no features of the UPO need ever be determined explicitly.

In some situations it may be impossible to produce a feedback signal that faithfully reproduces the form of Eq. (2) due to the latency of the control loop. As a rough guideline, the latency becomes an issue when the time lag t_ℓ through the loop is comparable to or larger than the correlation time of the chaotic system which is approximately equal to λ^{-1} , where λ is the largest (local) positive Lyapunov exponent of the desired UPO in the absence of control. Under conditions when the latency is important, the actual adjustments of the system parameter is given by $\delta p_{actual}(t) = \delta p(t-t_\ell)$.

B. Linear stability analysis of ET DAS feedback control

The control parameters γ and R can be determined empirically in an experiment or by performing a linear stability analysis of the system in the presence of ET DAS feedback control for fixed $\hat{\mathbf{n}}$ and \bar{p} . Such an analysis can yield important information about the possible effects of control on a system, such as identifying the orbits that may be controlled, and the range (if any) of feedback gain needed to achieve control for a particular R . Briefly, the analysis proceeds by considering a system described by

$$\dot{\mathbf{x}}(t) = \mathbf{f}(\mathbf{x}(t), t; p), \quad (3)$$

$$p = \bar{p} + \delta p(t),$$

where the ET DAS feedback signal $\delta p(t)$ [given by Eq. (2)] is included as a perturbation to the parameter \bar{p} . For simplicity, we consider the case where the latency of the control loop can be ignored ($t_\ell = 0$).

Following Ref. 10 we consider small perturbations $\mathbf{y}(t) = \mathbf{x}(t) - \mathbf{x}_*(t)$ about a τ -periodic orbit $\mathbf{x}_*(t)$. The dynamics of the perturbations in a neighborhood of the orbit are governed by

$$\dot{\mathbf{y}}(t) = \mathbf{J}(t) \cdot \mathbf{y}(t) - \gamma \mathbf{M}(t) \cdot \left[\mathbf{y}(t) - (1-R) \times \sum_{k=1}^{\infty} R^{k-1} \mathbf{y}(t-k\tau) \right], \quad (4)$$

where $\mathbf{J}(\mathbf{x}_*(t)) \equiv \partial \mathbf{f} / \partial \mathbf{x} |_{\mathbf{x}_*(t), \bar{p}}$ is the Jacobian of the uncontrolled system and $\mathbf{M}(\mathbf{x}_*(t)) \equiv (\partial \mathbf{f} / \partial \mathbf{p} |_{\mathbf{x}_*(t), \bar{p}}) \otimes \hat{\mathbf{n}}$ is an $m \times m$ dyadic that contains all information about how the control is applied to the system and how small changes in p affect it. The general solution to Eq. (4) can be decomposed into a sum of periodic functions (modes) with exponential envelopes. The growth of an exponential envelope in a period τ is quantified by its Floquet multiplier μ which can be found from the modified eigenvalue equation

$$\left| \mu^{-1} \mathbf{T} \left[\exp \int_0^\tau \left(\mathbf{J}(t) - \gamma \frac{1-\mu^{-1}}{1-\mu^{-1}R} \mathbf{M}(t) \right) dt \right] - \mathbf{1} \right| = 0, \quad (5)$$

where the time-ordered product notation $\mathbf{T}[\dots]$ represents the operator which advances $\mathbf{y}(t)$ forward in time by an amount equal to τ , and $\mathbf{1}$ is the identity matrix. In general, the time-ordered product cannot be obtained analytically, although it can be found using numerical techniques. To simplify our discussion, we denote the left-hand-side of Eq. (5) by $g(\mu^{-1})$. We note that g has an infinite number of roots, corresponding to the infinite number of modes introduced by the time delay.

An UPO is linearly stable under ET DAS control for a given set of parameters if and only if all the Floquet multipliers lie inside the unit circle in the complex plane, that is, if $|\mu| < 1$ for all μ satisfying Eq. (5). Equivalently, the system is stable if and only if g has no roots on the unit disk since $g(\mu^{-1})$ has no poles on the unit disk. The number of roots of $g(\mu^{-1})$ on the unit disk can be determined by counting the number of times $g(\mathbf{z})$ winds around the origin as \mathbf{z} traverses the unit circle. A necessary and sufficient condition for linear stability of the UPO in the presence of ET DAS feedback control is that this winding number vanish.

In a typical situation, the choice of accessible system parameter p and the number of system variables that can be measured is restricted, both by physical principles and practical considerations. Thus, one wishes to map out the domain of values of γ and R for which ET DAS is successful for a given p and $\hat{\mathbf{n}}$ over some range of values of a bifurcation parameter. In principle, $\mathbf{J}(t)$ and $\mathbf{M}(t)$ can be estimated from

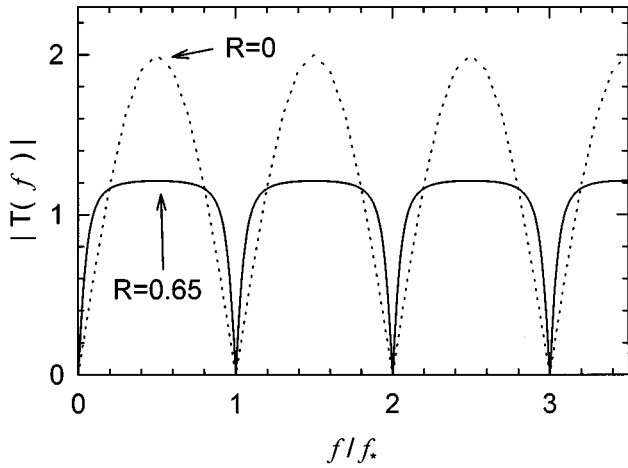


FIG. 3. Transfer function $|T(f)|$ of ETDAS feedback. The dashed line is for $R=0$ and the solid line is for $R=0.65$. Note that notches at $f/f_* = q$ ($q=0,1,2,\dots$) are narrower for $R=0.65$.

experimental data. This may not be practical, however, especially in high-speed systems. It is therefore important to compare theoretical predictions and experimental observations for simple systems in which accurate model equations are available so as to reveal qualitative features that should be kept in mind when trying to find a stable regime in a less well characterized system. We note that an approximate stability analysis of Eq. (3) has been undertaken recently.³⁹

C. Frequency domain analysis of ETDAS feedback

While the time-domain stability analysis outlined above gives a complete picture of ETDAS feedback in a neighborhood of the UPO, a frequency-domain analysis helps clarify the underlying reasons for its effectiveness in stabilizing highly unstable orbits as $R \rightarrow 1$. Note that the ETDAS feedback signal given by Eq. (2) linearly relates the input signal $\xi(t)$ with the output signal $\delta p(t)$; hence $\delta p(f) = -\gamma T(f)\xi(f)$, where $\xi(f)$ and $\delta p(f)$ are the Fourier amplitudes of the input and output signals, respectively, and

$$T(f) = \frac{1 - \exp(i2\pi f\tau)}{1 - R\exp(i2\pi f\tau)}, \tag{6}$$

is the transfer function for ETDAS feedback. The transfer function ‘filters’ the observed state of the dynamical system, characterized by $\xi(f)$, to produce the necessary feedback signal.

Figure 3 shows the frequency dependence of $|T(f)|$ for $R=0$ (TDAS) and $R=0.65$ (ETDAS) where it is seen that there are a series of notches that drop to zero at multiples of the characteristic frequency of the orbit $f_* = \tau^{-1}$ and that the notches become narrower for larger R . The existence of the notches in the transfer function can be understood easily by considering that $\delta p(t)$, and hence $\delta p(f)$, must vanish when the UPO is stabilized. Recall that the spectrum $\xi(f)$ of the system when it is on the UPO consists, in general, of a series of δ -functions at multiples of the characteristic frequency of the orbit $f_* = \tau^{-1}$; therefore, the filter must remove these

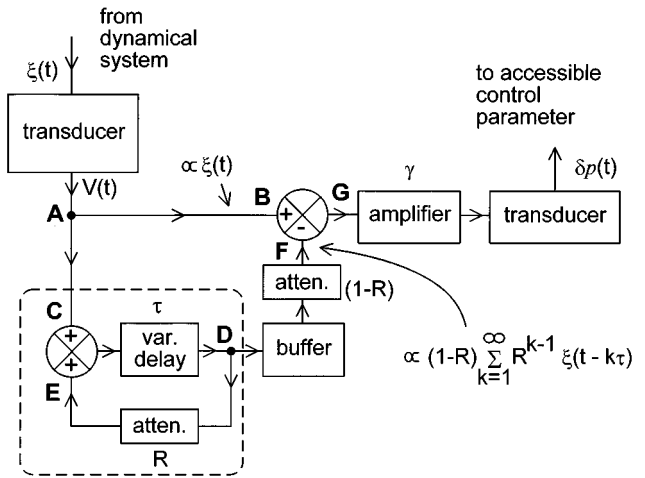


FIG. 4. One possible implementation of ETDAS feedback. The setup generates the feedback signal $\delta p(t)$ by combining the measured state variable of the system $\xi(t)$ with an infinite series of values of the state variable delayed in time by integral multiples of the period τ of the desired UPO. The dashed box contains the components that generate the infinite delayed series. This delayed series is subtracted (point F) from the current value of the system state variable (point B), amplified, then converted to the feedback signal $\delta p(t)$.

frequencies (via the notches) so that $\delta p(f) = 0$. The ETDAS feedback is more effective in stabilizing UPOs for larger R partly because it is more sensitive to frequencies that could potentially destabilize the UPO. The narrower notches imply that more feedback is generated for signals with frequency components slightly different from the desired set. In addition, $|T(f)|$ is flatter and remains near one between the notches for larger R , so the system is less likely to be destabilized by a large feedback response at these intermediate frequencies.

We note that other transfer functions that possess notches at multiples of f_* could stabilize the dynamics of the UPO; however, Eq. (6) is easy to implement experimentally.

IV. IMPLEMENTATION OF ETDAS

A. General implementation

ETDAS feedback control of UPOs can be implemented straightforwardly using a variety of techniques, even on fast time-scales. One possible logical design of the feedback loop is shown schematically in Fig. 4. We assume for the moment that the components impart negligible propagation delays on the various signals (except, of course, for the intentional delay τ necessary to form the ETDAS feedback signal). The dynamical state of the system $\xi(t)$ is converted to a voltage $V(t)$ by a transducer. The power of this signal is split equally between two different paths (point A); half of the signal is directed to one input port (point B) of a voltage subtraction device and is related to the first term on the right-hand-side of Eq. (2); the other half is directed to one input port (point C) of a voltage addition device forming part of the group of components (dashed box) generating the delay terms in Eq. (2). The signal in the latter path emerges from the addition device, propagates through a variable delay line with the

delay time set equal to the period τ of the desired UPO (point **D**), is attenuated by an amount R , and is injected into the second port (point **E**) of the addition device where it is combined with the original signal. A high-impedance buffer senses the voltage signal at the output of the delay line (point **D**). The signal emerging from the buffer is attenuated by $(1 - R)$, injected into the second port (point **F**) of the voltage subtraction device, and represents the second term on the right-hand-side of Eq. (2). The signal emerging from the subtraction device (point **G**) is proportional to the ETDAS error signal; it is amplified and injected into a transducer that adjusts the accessible control parameter by $\delta p(t)$. We note that all of the operations performed by the components between the input and output transducers could be accomplished entirely with a digital computer equipped with analog-to-digital and digital-to-analog converters, if the dynamics of interest were slow enough.

We emphasize that the unavoidable propagation delays through components must be thoroughly characterized in any real implementation of ETDAS. As described in Sec. IV C, small additional time delays must be added to the feedback system and adjustments must be made to compensate for the time delays inherent in the components.

B. All-optical implementation

One useful feature of ETDAS feedback is the ability to generate the error signal using an all-optical technique.^{8,34,35,40} Specifically, the form of the ETDAS error signal given by Eq. (2) is identical to an equation that describes the reflection of light from a Fabry-Perot interferometer⁴¹ consisting of two equal-reflectivity mirrors, where $R = r^2$ corresponds to the square of amplitude-reflection-coefficient r of the mirrors, and τ corresponds to the round-trip transit-time of light in the cavity. In one possible scenario, the input transducer shown in Fig. 4 generates a laser beam of field strength $E_{inc}(t)$ that is directed toward an optical attenuator or amplifier (controlling γ) and a Fabry-Perot interferometer as shown in Fig. 5. The field $E_{ref}(t)$ reflected by the interferometer passes through the attenuator/amplifier and is converted to the ETDAS error signal $\delta p(t)$ by the output transducer. It may be possible to control fast dynamics of optical systems that generate directly a laser beam, such as semiconductor diode lasers, using the field generated by the laser as the measured system parameter $\xi(t)$ and as the accessible system parameter $\delta p(t)$; no transducers are required.^{8,34,35,40}

C. Specific implementation for controlling the fast diode resonator

1. Electronic circuit layout

We control the dynamics of a fast chaotic electronic circuit known as a diode resonator, described in the next section, using an analog-electronic implementation of ETDAS as shown schematically in Fig. 6. The implementation attempts to mimic as closely as possible the generic design described in Sec. IV A. It balances considerations of the finite propagation time of the signals through the components (affecting the control-loop latency), distortion of the signals

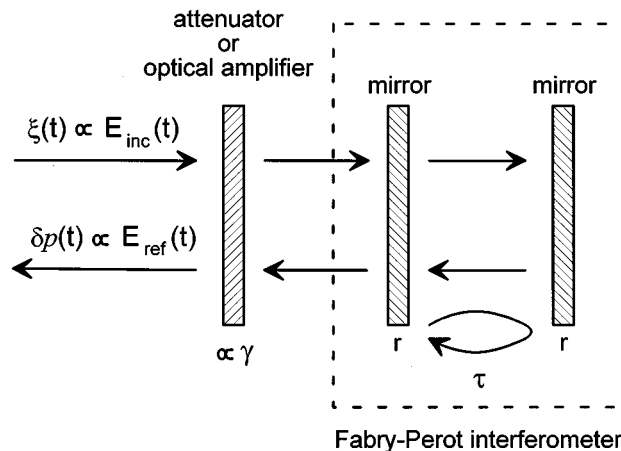


FIG. 5. All-optical implementation of ETDAS feedback using a Fabry-Perot interferometer consisting of two mirrors with amplitude reflection coefficient r separated by a distance such that the round-trip-time of light in the cavity is equal to the period τ of the desired UPO. An optical attenuator or amplifier adjusted the feedback gain γ .

(affecting the fidelity of the feedback signal), and noise, with the simplicity of the layout, ease of construction, and price. No transducers are required in this design because the accessible system parameter, denoted by $V(t)$, and control parameter, denoted by $V_{\delta p}(t)$, are voltage signals.

The electrical signals propagate through the circuit in a fashion similar to that described in Sec. IV A for the generic implementation of ETDAS; points (**A-F**) in Fig. 6 for the specific implementation correspond to the same points in Fig. 4 for the generic implementation. One goal of the circuit layout shown in Fig. 6 is to ensure that the difference in propagation time of signals from points **A**→**G'** and **A**→**D'**→**D**→**F**→**G'** is equal to τ and the time from **D**→**E**→**D'**→**D** is also equal to τ in order to faithfully produce the ETDAS error signal. This task is complicated by the nonzero propagation delays through the electronic components.

In our layout, the accessible system parameter $V(t)$ is sensed by a high-impedance buffer (**B1**) and the power associated with this signal is split equally between two different paths (point **A**). Half of the signal is directed to the input (point **B**) of an inverting, summing operational amplifier (**A1**) and the other half is directed to the input (point **C**) of a second inverting, summing amplifier (**A2**) where it is filtered with predistortion circuitry (**F1**). The signal emerging from **A2** propagates through a long, variable delay line (**D1**) with a delay time set close to, but less than, the period τ of the desired UPO, is inverted and amplified (**A3**) by a fixed amount to compensate for the average loss of the delay line, passes through a short variable delay line (**D2**), attenuated to set the control parameter R , and directed to the input (point **E**) of **A1** where it is filtered with predistortion circuitry (**F2**). The signal emerging from the long delay line (point **D**) is sensed with a noninverting amplifier (**A4**), passes through a short variable delay line (**D3**, point **F**), and is directed to the input of the summing amplifier **A1** where it is attenuated by a factor equal to $(1 - R)$ by adjusting **P1**. The signal emerg-

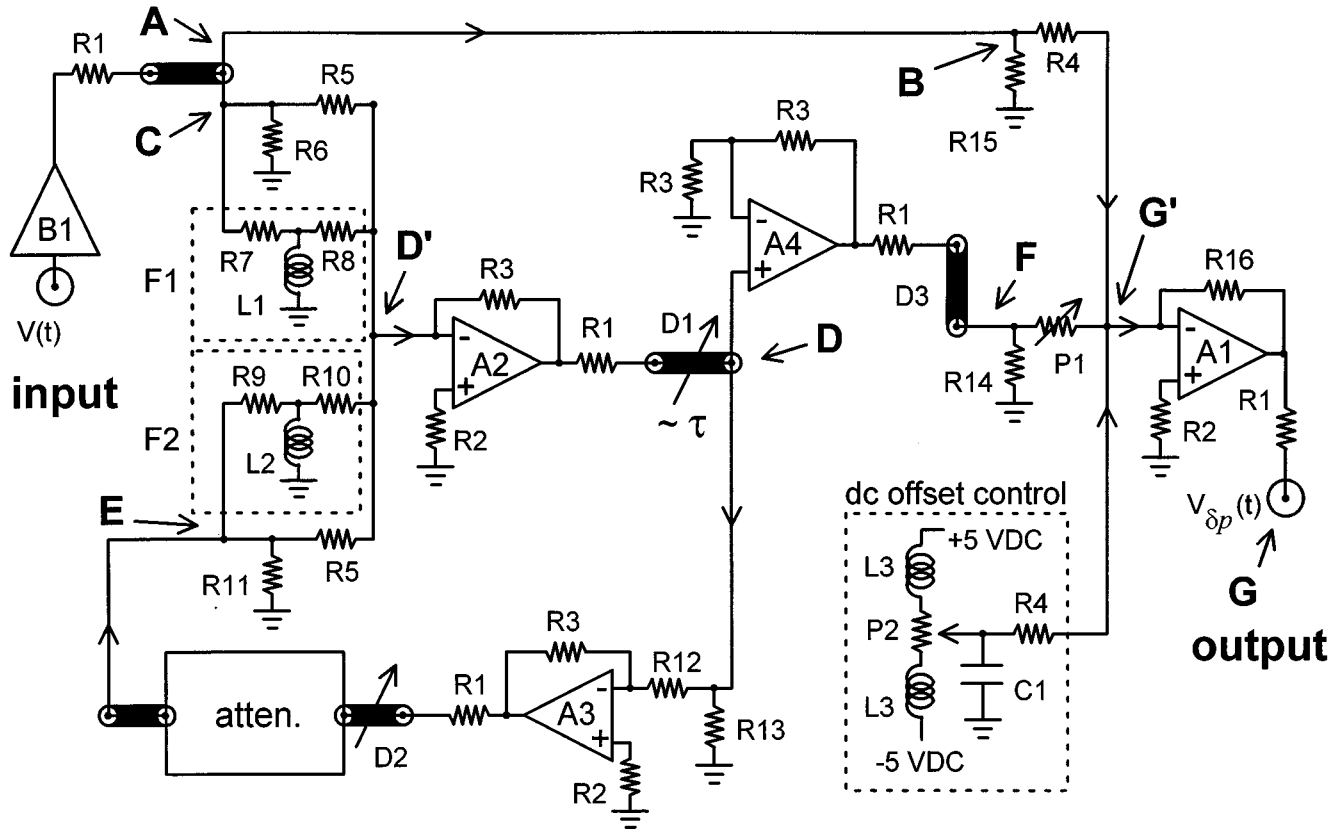


FIG. 6. Specific implementation of the ETDAS feedback circuitry for controlling the dynamics of a high-speed diode resonator. The signal $V(t)$ is combined with an infinite series of previous values delayed by multiples of the orbital period τ . The dashed box marked 'dc offset control' compensates for small offsets introduced by the circuitry. A1–A4 are operational amplifiers, B1 is a high-impedance buffer, and D1–D3 are delay lines. The dashed boxes F1 and F2 contain predistortion filters; their components depend on the particular choice of delay cable D1. Component values are: For stabilizing the period-1 UPO, $L1 = 0.33 \mu\text{H}$, $L2 = 0.33 \mu\text{H}$, $R7 = 150 \Omega$, $R8 = 402 \Omega$, $R9 = 100 \Omega$, $R10 = 825 \Omega$; for the period-4 UPO, $L1 = 1.0 \mu\text{H}$, $L2 = 1.0 \mu\text{H}$, $R7 = 150 \Omega$, $R8 = 590 \Omega$, $R9 = 100 \Omega$, $R10 = 1540 \Omega$. Other component values are: $C1 = 0.1 \mu\text{F}$, $L3 = 3.3 \mu\text{H}$, $P1 = 5 \text{ k}\Omega$, $P2 = 1 \text{ k}\Omega$, $R1 = 50 \Omega$, $R2 = 100 \Omega$, $R3 = 715 \Omega$, $R4 = 499 \Omega$, $R5 = 357 \Omega$, $R6 = 255 \Omega$, $R11 = 140 \Omega$, $R12 = 324 \Omega$, $R13 = 59 \Omega$, $R14 = 53.6 \Omega$, $R15 = 215 \Omega$, and $R16 = 1 \text{ k}\Omega$.

ing from A1 (point G) is proportional to the ETDAS error signal; it is directed to additional amplifiers to set the feedback gain γ and injected into the diode resonator.

2. Selection of components

One primary issue in designing the ETDAS circuitry is minimizing the control-loop latency t_{ℓ} . The latency must be much less than $\sim 100 \text{ ns}$ to control the diode resonator described in the next section based on our estimate of the values of the conditional Lyapunov exponents characterizing the UPOs. In this proof-of-principle investigation of ETDAS, we select commercially available, inexpensive operational amplifiers and buffers which add very little to t_{ℓ} yet are easy to obtain and incorporate into the design. For our choice of components, $t_{\ell} \sim 10 \text{ ns}$. Smaller latencies may be possible using custom-built microwave circuitry; we do not explore this option.

The control-loop latency is governed by the time it takes for the signal to propagate from the input to the output of the ETDAS following the path A \rightarrow B \rightarrow G since the portion of the signal at G should be proportional ideally to the input signal (with no time lag). Propagation delays of the signal

passing through the other components forming the infinite series of time-delay terms is not as important because they can be compensated using a slightly shorter coaxial cable (D1). We select the AD9620 (Analog Devices,⁴² propagation delay $\approx 1 \text{ ns}$, bandwidth 600 MHz) for B1 and the AD9618 (Analog Devices, propagation delay $\approx 3 \text{ ns}$, bandwidth 160 MHz) for A1 because they have short propagation delays, are relatively easy to use, and are low cost. In the other parts of the circuit where propagation delays are not as important (A2–A4), we select the AD811 (Analog Devices, propagation delay $\approx 6 \text{ ns}$, bandwidth 140 MHz) because its stability is less sensitive to the precise layout of the components. Note that the bandwidth of all components is significantly larger than the characteristic frequency of the chaotic system (10.1 MHz), thereby minimizing the distortion of the ETDAS feedback signal. Operational amplifiers and buffers with similar or better specifications should produce similar results.

Due to the high bandwidth of these devices, we use standard high-frequency analog electronic techniques. The components are laid out on a home-made, double-sided printed circuit board in which the signal traces form a transmission

line (nominal impedance 50 Ω) and are kept under 2 cm, proper ground planes are maintained under all components, and PC board mounted SMA jacks are used to transfer the signals from the board to coaxial cables. The printed circuit boards are fabricated in a multi-step process: We create a graphical layout of the traces using a simple drawing program on a personal computer; the drawing is printed on a 'transfer film' with a laser printer;⁴³ the traces are transferred to the clean, bare copper surface of the board; the plastic backing of the transfer film is removed; the board is etched using a hot ammonium persulfate solution; holes are drilled for the leads of the components; and the components are soldered to the board. The power supply leads to all operational amplifiers are bypassed with ceramic and tantalum capacitors as close as possible to the power supply pins, and ferrite beads isolate the power supply lines between components. The dc offset voltage of the amplifiers is compensated at the last stage of the circuitry (point \mathbf{G}') by adding a dc voltage to the signal from a filtered, adjustable power supply, as shown in Fig. 6. All signals routed between the ETDAS and other circuit boards propagate through short 50 Ω coaxial cables (type RG-58/U).

Another primary issue in the implementation of ETDAS feedback is minimizing the distortion (frequency-dependent attenuation and phase shift) of signals propagating through the coaxial delay line that sets the time delay τ . Previous implementations of TDAS have used for the delay line a variable length transmission line,⁸ electro-optic delay line,²⁸ or digital first-in-first-out delay device.²⁹ Distortion is difficult to avoid for the high-period UPOs because the delay line is long, and for the case when the feedback parameter $R \rightarrow 1$ since the signals circulates many times through the delay line. To minimize the distortion, we use low-loss, semi-rigid 50 Ω coaxial cable (1/4 in. HELIAX type FJSJ1-50A⁴⁴). We find that this delay line gives superior performance in comparison to standard coaxial cable (type RG-58/U). The attenuation characteristics of the HELIAX cable is 0.175 dB/100 ft. at 1 MHz and 1.27 dB/100 ft. at 50 MHz which should be compared to 0.33 dB/100 ft. at 1 MHz and 3.15 dB/100 ft. at 50 MHz for the RG-58/U cable.

3. Adjustment of circuit parameters

The final preparation step for controlling the dynamics of the chaotic system using ETDAS feedback is to adjust the time delay τ and the feedback parameter R . We note that setting τ requires adjusting the propagation time of signals following *two* different paths. Referring to Fig. 6, the difference in time it takes for signals to propagate from $\mathbf{A} \rightarrow \mathbf{B} \rightarrow \mathbf{G}'$ and from $\mathbf{A} \rightarrow \mathbf{D} \rightarrow \mathbf{F} \rightarrow \mathbf{G}'$ must be equal to τ . *In addition*, the propagation time around the delay loop ($\mathbf{D} \rightarrow \mathbf{E} \rightarrow \mathbf{D}' \rightarrow \mathbf{D}$) must also equal τ . Note that these times include the propagation time through all components: The coaxial cable, the amplifiers and attenuators, and the signal traces and connectors. The timing can be achieved straightforwardly using three coaxial delay lines: A long delay line $D1$ consisting of a HELIAX cable whose propagation time is close to but less than τ , a short coaxial cable (type RG-58/U) for fine tuning

the propagation time of $D1$, and a constant-impedance adjustable delay line (Hewlett-Packard model 874-LK10L⁴⁵) for ultra-fine adjustment of $D1$; a short variable delay line $D2$ consisting of another adjustable delay line and coaxial cables (type RG-58/U) whose length is just long enough to connect this variable delay line to the printed circuit board; and a short, fixed delay line $D3$.

Initial adjustment of the timing is achieved by injecting a weak sinusoidal voltage whose period is equal to τ at point \mathbf{A} . The first step is to adjust the circuitry for TDAS feedback ($R=0$), that is, to set the path difference between $\mathbf{A} \rightarrow \mathbf{B} \rightarrow \mathbf{G}'$ and $\mathbf{A} \rightarrow \mathbf{D} \rightarrow \mathbf{F} \rightarrow \mathbf{G}'$ to τ with the circulating loop temporarily disabled by disconnecting the attenuator (Kay Elemetrics model 1/839 manual step attenuator⁴⁶). The length $D1$ is set so that the sinusoidal signal at point \mathbf{F} is delayed by one period from the signal at point \mathbf{B} . The amplitude of the delayed signal is adjusted so that the signal at the output of the ETDAS circuitry (point \mathbf{G}) is minimized using the variable resistor PI ; iterating this procedure while monitoring the signal at \mathbf{G} results in precise adjustment of $D1$. Next, the circulating loop is reconnected with the attenuator set so that $R \sim 0.1$. The delay $D2$ and the variable resistor PI are adjusted to minimize the signal at \mathbf{G} . Sensitive adjustment of $D2$ is achieved by decreasing the attenuation so that $R \rightarrow 1$ and iterating the setting of $D2$ and PI . Typically, the 10.1 MHz sinusoidal input signal is suppressed at point \mathbf{G} by ~ 50 dB at 10.1 MHz.

Note that our procedure results in a ETDAS feedback signal $V_{\delta p}(t) = V_{\delta p}^{ideal}(t - t_{\ell})$, where $V_{\delta p}^{ideal}(t)$ is the ideal feedback signal in the absence of control-loop latency, and t_{ℓ} is the latency with contributions from the total time lag of the signal as it propagates from the diode resonator, through the ETDAS circuitry and additional amplifiers setting the feedback gain γ , and the summing amplifier that injects the feedback signal into the diode resonator.

Adjusting the feedback parameter R to any desired value is straightforward once the timing of the circuit is achieved. A new value of R is selected by setting the attenuator and adjusting the variable resistor PI which sets the value of $(1 - R)$ in Eq. (2).

4. Compensating for nonideal circuit behavior

We characterize the quality of the ETDAS circuitry by measuring its frequency-domain transfer function $|T(f)|$ (recall the ideal shape of $|T(f)|$ shown in Fig. 3). Figure 7 shows $|T(f)|$ for $\tau = 400$ ns corresponding to a fundamental frequency $f_{*} = 2.5$ MHz (for controlling the period-4 UPO of the diode resonator), $R=0$ (dashed line), and $R=0.65$ (solid line) where we adjust the circuit parameters so that the notch at 10 MHz is as close to zero as possible. We optimize the circuit for operation at 10.1 MHz, rather than 2.5 MHz because the spectrum of the period-4 orbit has a large peak at 10.1 MHz. It is seen that all other notches have a transmission less than 0.047 for $R=0.65$ and less than 0.017 for $R=0$. The agreement between the observed and predicted

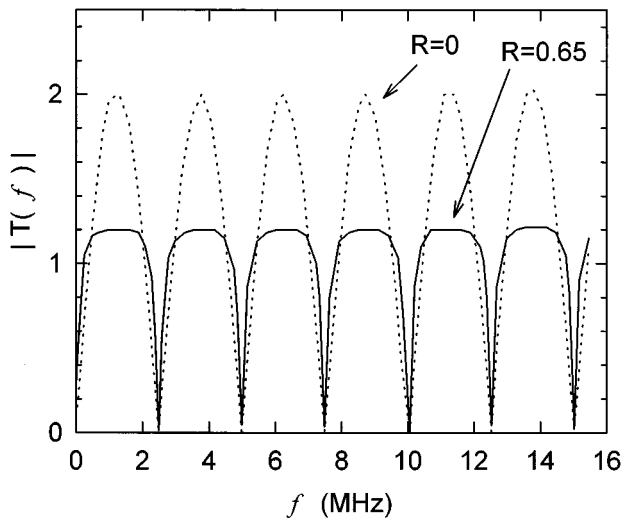


FIG. 7. Experimentally determined transfer function of the ETDAS circuitry shown in Fig. 6 for $R=0$ (dashed line), $R=0.65$ (solid line), and $\tau=400$ ns ($f_* \approx 2.5$ MHz).

behavior is very good, especially when one considers that the sensitivity of the shape of the notches on the distortion of the delay line increases as $R \rightarrow 1$.

We find that these high-quality results are only possible when the signals are filtered with predistortion circuitry (*F1* and *F2*) that attempt to cancel the small distortion caused by the HELIAX cable. The filters, consisting of two resistors and an inductor, do not significantly effect the signals at low frequencies and boost their amplitude a high frequencies in a fashion opposite to the small frequency dependent attenuation of the coaxial cable. For comparison, Fig. 8 shows $|T(f)|$ with the predistortion filters (*F1* and *F2*) removed

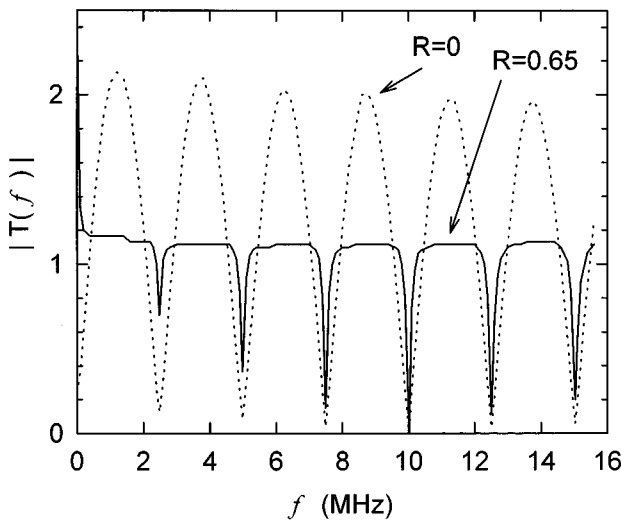


FIG. 8. Transfer function of the ETDAS circuitry shown in Fig. 6 with the predistortion filters removed for $R=0$ (dashed line), $R=0.65$ (solid line), and $\tau=400$ ns ($f_* \approx 2.5$ MHz). The fact that the notches do not drop to zero indicates the uncompensated distortion of the long delay line.

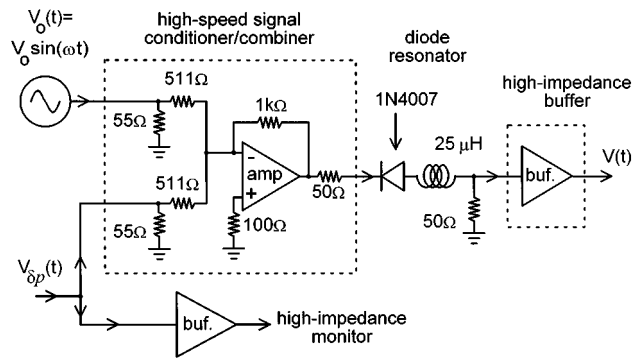


FIG. 9. The high-speed diode resonator. The series-connected rectifier diode, inductor, and resistor are driven by a leveled sinusoidal voltage $V_0(t)$. The signal conditioner/combiner isolates the driver from the circuit, and injects the feedback voltage $V_{\delta p}(t)$ into the diode resonator. A high-impedance buffer measures $V(t)$, which is proportional to the current flowing in the resonator.

where we make minor adjustments of the circuit parameters to optimize the notch at 10.1 MHz. It is seen that the performance of the device is severely degraded, especially for $R=0.65$. We note that acceptable behavior of the ETDAS feedback circuitry with $\tau=400$ and $R=0.65$ can not be obtained using standard coaxial cable (type RG-58/U) even with the predistortion filters.

V. CONTROLLING CHAOS IN A FAST DIODE RESONATOR USING ETDAS

A. The fast diode resonator

In our experimental studies of controlling chaos on fast time-scales, we use a ‘diode resonator’ because it displays a wide variety of nonlinear behaviors including period doubling bifurcations, hysteresis, intermittency, and crisis; it is easy to build and customize; and it is well characterized on slow time-scales.⁴⁷⁻⁵⁴ The low-speed diode resonator typically consists of an inductor and a diode connected in series, driven by a sinusoidal voltage.

The high-speed variation of the diode resonator, shown schematically in Fig. 9, has additional components needed to implement high-speed control. It consists of a rectifier diode (type 1N4007, hand-selected for low junction capacitance) in series with a $25 \mu\text{H}$ inductor (series DC resistance of 2.3Ω) and a resistor $R_s = 50 \Omega$ driven by a leveled sinusoidal voltage $V_0(t) = V_0 \sin(\omega t)$ ($\omega/2\pi \approx 10.1$ MHz) that passes through a high-speed signal conditioner (50Ω output impedance). The resistor R_s converts the current flowing through the diode resonator (the measured dynamical variable) into a voltage $V(t)$ which is sensed by a high-impedance buffer (Analog Devices AD9620, propagation delay ≈ 1 ns). The signal conditioner consists of a high-speed inverting amplifier (Analog Devices AD9618, propagation delay ≈ 3 ns) and serves two purposes: It isolates the sine-wave generator (Tektronix model 3325A⁵⁵) from the diode resonator and it combines the sinusoidal drive signal $V_0(t)$ with the ETDAS feedback signal $V_{\delta p}(t)$. The components are laid out on a home-made, double-sided printed circuit board in which the

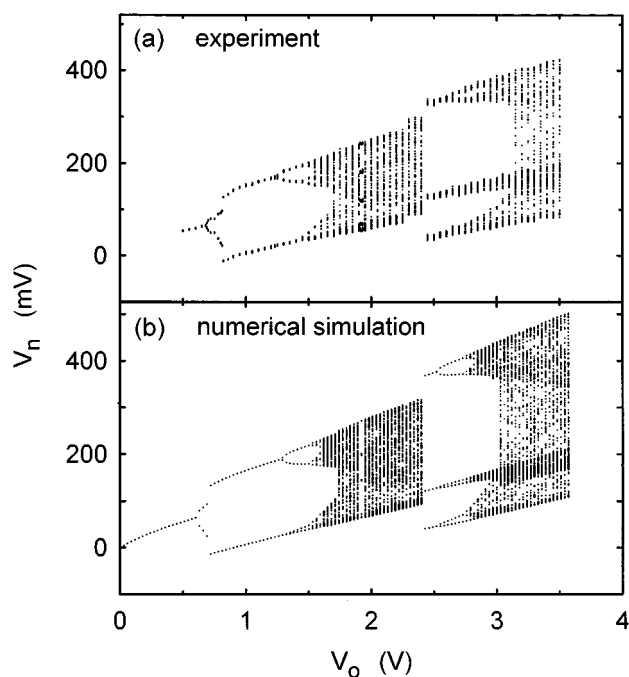


FIG. 10. Bifurcation diagrams of the diode resonator: Peak voltage V_n as a function of the drive amplitude V_0 . (a) Experimental data. (b) Numerical simulations.

traces are kept under 2 cm, proper ground planes are maintained under all components, and the signals entering or leaving the board pass from the traces to coaxial cables through PC board mounted SMA jacks. A high-impedance buffer (Analog Devices AD9620) is also included to monitor the ETDAS feedback signal. We find that it is crucial to incorporate the current-to-voltage converter (the 50Ω resistor) into the architecture of the chaotic oscillator to minimize the latency of the loop; we believe that incorporating some components of the feedback loop into the chaotic system must be considered when attempting to control any high-speed dynamics.

We record a bifurcation diagram and first-return maps to characterize the dynamics of the uncontrolled diode resonator using the sinusoidal drive amplitude V_0 as the bifurcation parameter. In the experiments, we capture multiple (typically three) $40\text{-}\mu\text{s}$ -long time-series data of $V(t)$ using a 100 MHz, 8-bit digitizing oscilloscope (Tektronix model 2221A) and determine the maxima of $V(t)$, denoted by V_n , using a second-order numerical interpolation routine. The bifurcation diagram [Fig. 10(a)] is generated by plotting approximately 300 values of V_n for each value of V_0 as it is varied from small to larger values (hysteresis in the system is evident when V_0 is varied from the largest to smaller values of V_0 , but it is not shown in this diagram for clarity). It displays a typical period-doubling cascade to chaos where the transition to chaos occurs at $V_0 \approx 1.5$ V. Also evident are a narrow period-5 periodic window at $V_0 \approx 1.8$ V and a large period-3 window starting at $V_0 \approx 2.4$ V. The first-return maps are generated by plotting V_n vs. V_{n+1} for fixed values of V_0 . The experimentally observed chaotic maps of the system be-

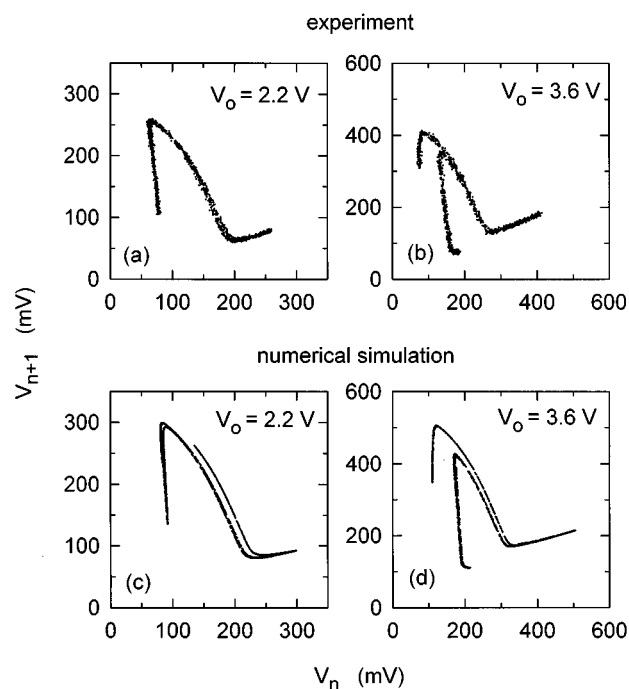


FIG. 11. First return maps of the unperturbed diode resonator above and below the period-3 window. Experimental maps (a) $V_0=2.2$ V and (b) $V_0=3.6$ V are in good agreement with numerically simulated maps (c) $V_0=2.2$ V and (d) $V_0=3.6$ V.

low ($V_0=2.2$ V) and above ($V_0=3.6$ V) the period-3 window are shown in Figs. 11(a) and (b), respectively. The general structure of these maps are similar to observed in low-frequency diode resonators.⁵³

Considering the complexity associated with predicting theoretically the stability of the high-speed diode resonator in the presence of ETDAS feedback based solely on experimental measurements, we use a simple model of the resonator that captures the essence of its behavior. The model, described briefly in the Appendix, treats the real components of the resonator as collections of ideal components in a fashion similar to that used in commercially available electronic simulation software packages. All parameters of the model are determined by independent measurements of the components. We find very good agreement between the experimentally observed and numerically generated bifurcation diagrams [Fig. 10(b)] and first-return maps [Figs. 11(a) and (b)]. It is seen that all features observed in the experiment are predicted by the model; however, there is a slight discrepancy in the location of the periodic windows and in the size of V_n . As we will see in Sec. V F, this model is adequate to predict with good accuracy the stability of the controlled resonator.

B. Experimental observation of control

Our procedure for achieving control of the high-speed diode resonator using ETDAS is to: set the delay-time τ , the feedback parameter R , and optimize the feedback circuitry off-line as described in Sec. IV C 3; connect the ETDAS

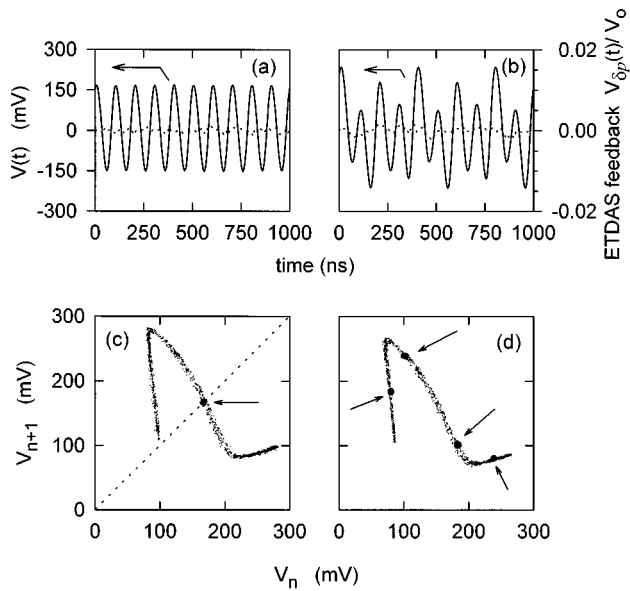


FIG. 12. Time series data and first return maps illustrating successful ETDAS control. Temporal evolution (solid lines, scale on left) of the stabilized (a) period-1 UPO ($\gamma=6.2$, $R=0.28$) and (b) period-4 UPO ($\gamma=4.2$, $R=0.26$) along with their associated ETDAS error signals $V_{\delta p}(t)$ (dashed lines, scale on right), expressed as a fraction of the drive amplitude. Similar data in the form of a first return map for the controlled (c) period-1 ($\gamma=4.4$, $R=0$) and (d) period-4 ($\gamma=3.1$, $R=0.26$) trajectories are highlighted by the dark concentrations of points indicated by arrows. These maps are superimposed on maps of the uncontrolled chaotic resonator. For (a)-(d), $V_0=2.4$ V.

circuitry to the diode resonator using short coaxial cables; and search for control while adjusting the feedback gain γ . Control is successful when $V(t)$ is periodic with the desired period τ and the magnitude of the feedback signal $V_{\delta p}$ drops below a level set by $|T(f)|$ (the transmission of the worst notch) and the noise level in the system. In principle, $V_{\delta p}$ vanishes in an ideal situation. In practice, noise and nonideal behavior of the ETDAS circuitry (see Sec. IV C 4) lead to a nonzero value of $V_{\delta p}(t)$. Our criterion for control is that $|V_{\delta p}(t)| < 5 \times 10^{-3} V_0$, or that $20 \log(|V_{\delta p}(t)|/V_0) < -46$ dB. We verify that the controlled orbits are indeed UPOs of the chaotic system to within the experimental uncertainty when this criterion is fulfilled by comparing the return maps of the controlled and uncontrolled systems. We note that periodic states that are not UPOs of the system can be obtained under different experimental conditions; in this case the feedback signal is large (of the order of V_0).

Figures 12(a) and (b) show the temporal evolution of $V(t)$ when the ETDAS feedback circuitry is adjusted to stabilize the period-1 and period-4 UPOs, respectively, together with the associated feedback signal. The sinusoidal drive amplitude is 2.4 V (the system resides in the chaotic regime just below the period-3 window in the absence of control) and the feedback parameters are $\gamma=6.2$, $R=0.28$ for the stabilized period-1 orbit and $\gamma=4.2$, $R=0.26$ for the period-4 orbit. It is seen that the feedback signal is a small fraction of the drive amplitude ($< 2 \times 10^{-3}$ for both cases). The slight increase in $V_{\delta p}(t)$ for the period-4 orbit is mainly due to

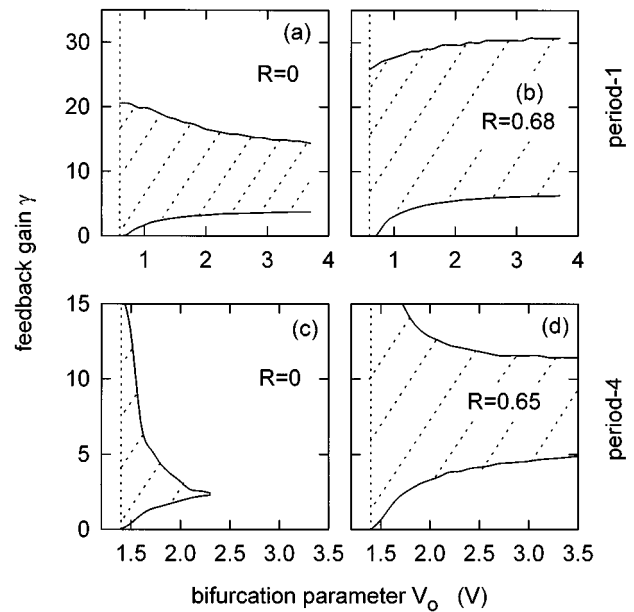


FIG. 13. Experimental domains of control as a function of the drive amplitude V_0 for period-1 and period-4 UPOs for two different values of R . The shaded regions illustrate period-1 domains of control for $R=0$ (a) and $R=0.68$ (b), and period-4 domains of control for $R=0$ (c) and $R=0.65$ (d). The dashed vertical lines mark the points at which the orbit becomes stable in the absence of feedback.

imperfect reproduction of the form of the ETDAS feedback signal by our circuitry. This effect is more prevalent for the period-4 setup because the delay line is longer and hence causes more distortion of the signals due to the dispersion and frequency-dependent loss of the coaxial cable.

Figures 12(c) and (d) presents further evidence that the ETDAS feedback indeed stabilizes the UPOs embedded within the strange attractor of the diode resonator. We show the return maps for the uncontrolled system (light dots) and the controlled system (dark dots indicated by arrows) for the stabilized period-1 orbit [Fig. 12(c), $R=0$, and $\gamma=4.4$] and the period-4 orbit [Fig. 12(d), $R=0.26$, and $\gamma=3.1$] for $V_0=2.4$ V. It is clear that the stabilized orbits lie on the unperturbed map, indicating that they are periodic orbits internal to the dynamics of the uncontrolled system.

C. Domain of control

We find that these UPOs can be stabilized using a wide range of feedback parameters which can be visualized quickly from a plot of the ‘domain of control.’ The domain of control is mapped out by determining the range of values of the feedback gain γ that successfully stabilizes an UPO as a function of the bifurcation parameter V_0 for various values of the feedback parameter R . In general, increasing the feedback parameter R tends to enlarge the domain of control and shift it to slightly larger values of γ . We find that the period-1 orbit can be stabilized using ETDAS feedback for all V_0 when $R=0$ and $R=0.68$ as seen in Figs. 13(a) and (b), respectively. It is clear that the range of γ that successfully

stabilizes the orbit for a given value of V_0 increases significantly for $R=0.68$ in comparison to $R=0$, especially for larger values of V_0 .

The largeness and shape of the domain of control is important for several practical reasons. Since the domain is large, the system is rather insensitive to drift in the feedback parameters or the state of the chaotic system, and control can be obtained even with imprecise, *a priori* knowledge of the proper feedback parameters. Also, the ETDAS feedback can automatically track changes in V_0 over its entire range without adjusting γ because the shape of the domain is a wide, horizontal band.

Increasing the size of the feedback parameter R gives rise to more dramatic effects on the domain of control when stabilizing the period-4 orbit, as shown in Figs. 13(c) and (d). It is seen that TDAS feedback ($R=0$) fails for moderate and larger values of the bifurcation parameter. The domain of control can be extended to include the entire range of V_0 using $R=0.65$, illustrating the superiority of ETDAS for controlling highly unstable orbits. Also, the size and shape of the domain of control for this case has all of the advantages mentioned in the previous paragraph for the period-1 domain of control.

D. Transient behavior

We find that the period-1 and period-4 UPOs shown in Fig. 12 can be stabilized by initiating control at an arbitrary time; we do not have to wait for the system to naturally approach the neighborhood of the UPO nor target the system to the UPO before control is initiated. Such control is possible for several reasons: The system is particularly simple in that there is only one period-1 and one period-4 UPO; the basin of attraction of these UPOs in the presence of ETDAS feedback is large; and we apply large perturbations [$V_{dp}(t)$ is comparable to $V_d(t)$] to the system during the transient phase.

The dynamics during the initial transient can be quite rich; the nature of the convergence of the system to the UPO is a function of the precise state of the system when control is initiated and the value of the control parameters. When the control parameters are adjust such that the system is near, but within, the domain of control, the system often displays brief intervals of periodic behavior other than the desired behavior during the transient phase. Figures 14(a) and (b) are two examples of the approach to the period-1 UPO for $V_0=1.9$ V, $R=0.68$, and $\gamma=5.2$ (a) or $\gamma=7.0$ (b), where we plot the peak value V_n of $V(t)$ as a function of the peak number n (control is initiated near $n=0$). In one case [Fig. 14(a)], an initial chaotic transient gives way to a period-2 behavior that decays exponentially to the desired UPO. In the second [Fig. 14(b)], an initial chaotic transient abruptly switches to controlled behavior.

Richer transient dynamics is observed when stabilizing the period-4 UPO, as shown in Figs. 14(c) and (d) for $V_0=1.9$ V, $R=0.26$, and $\gamma=6.1$ (c) or $\gamma=2.6$ (d). In one case [Fig. 14(c)], we observe a brief interval of period-2 behavior that eventually destabilizes and decays in an oscil-

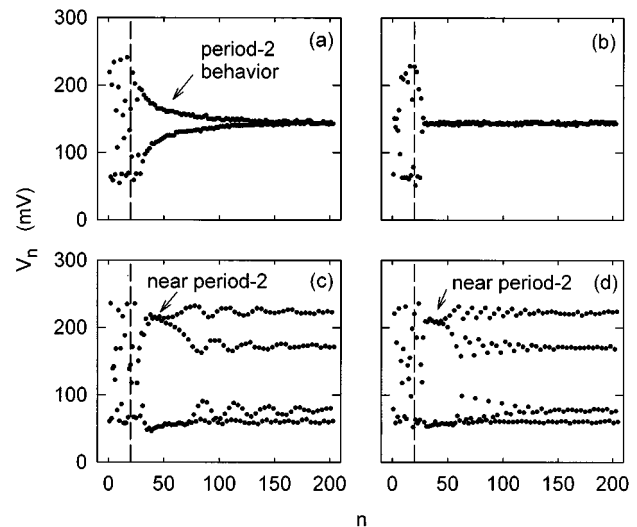


FIG. 14. Transient behavior of the diode resonator following initiation of ETDAS control. The dots represent the peak values V_n of $V(t)$. The dashed vertical line marks the point at which control is initiated. Convergence to a controlled period-1 UPO for $V_0=1.9$ V, $R=0.68$, (a) $\gamma=5.2$ and (b) $\gamma=7.0$. In addition, we show two approaches to the period-4 UPO for $V_0=1.9$ V, $R=0.26$, (c) $\gamma=6.1$ and (d) $\gamma=2.6$. Note that the transients have brief sections of decaying periodic behavior.

latory fashion to the desired UPO. In the other case [Fig. 14(d)], the system passes through intervals of period-2 and period-16 behavior before converging to the period-4 UPO. It is not surprising that the system resides near a period orbit with a period longer than the desired UPO since the ETDAS feedback cannot distinguish between the two different behaviors. However, the low-period behavior is not stable for long times since the ETDAS feedback is not sensitive to and does not correct for noise and fluctuations that destabilize this undesired low-period orbit.

E. Average time to attain control

While the transient dynamics are quite rich near the boundary of the domain of control, ETDAS feedback stabilizes rapidly the desired UPO over most of the domain. Figure 15 shows the average time $\langle t_r \rangle$ to obtain control of the period-1 UPO from an arbitrary starting time as a function of the feedback gain γ for $V_0=1.9$ V and $R=0$ [Fig. 15(a)] and $R=0.68$ [Fig. 15(b)]. The hashed region indicates the range of γ over which stable period-1 behavior is not observed. The data points represent the average of 20 trials and the error bars indicate the standard deviation of the times to obtain control. It is seen that $\langle t_r \rangle$ is less than $3 \mu\text{s}$ and typically less than $1 \mu\text{s}$ (10 orbital periods), except near the edge of the domain of control where $\langle t_r \rangle$ grows rapidly. In addition, it is seen that the range over which rapid control is obtained increases significantly by increasing R to 0.68. This highlights one of the advantages of ETDAS feedback control over TDAS feedback. Figures 16(c) and (d) show similar data for the period-4 UPO. We note that $\langle t_r \rangle$ should increase rapidly near the edges of the domain of control for this UPO (as it does in the period-1 case). In our experiment, however,

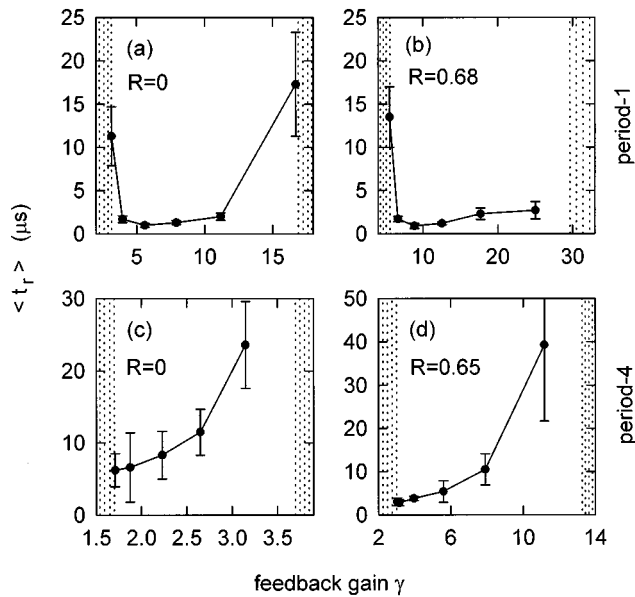


FIG. 15. Average transient times $\langle t_r \rangle$ as functions of feedback gain γ for the period-1 orbit with $V_0=1.9$ V and $R=0$ (a) and $R=0.68$ (b), and the period-4 transient times for $V_0=1.9$ V and $R=0$ (c) and $R=0.65$ (d). The error bars indicate the standard deviation of $\langle t_r \rangle$ and the hashed regions indicate the range of γ for which control is not obtained.

limited precision in γ makes it impossible to get sufficiently close to the low-gain boundary to detect the rapid increase.

F. Theoretical analysis

We find that the experimentally measured domains of control can be predicted theoretically with good accuracy using the techniques described in Sec. III B. Briefly, the procedure to determine the domain is to:¹⁰

- determine the trajectory of the desired UPO for one value of the bifurcation parameter V_0 by analyzing the coupled nonlinear differential equations describing the dynamics of the diode resonator [see Eq. (A4)];
- choose the feedback parameters $\hat{\mathbf{n}}$ and R (note that $\hat{\mathbf{n}}$ is set throughout the experiment by our choice of accessible system variable and control parameter);
- find the boundaries of the domain of control [the points at which the winding number jumps from zero to a positive integer, see Eq. (5)] for one value of the bifurcation parameter V_0 using standard numerical root-finding algorithms;
- follow the boundary by repeating this procedure for the other values of V_0 .

Note that this analysis does not include the effects of control-loop latency.

We compare the observed [Fig. 16(a)] and predicted [Fig. 16(b)] domain of control for the period-1 UPO when $R=0.68$. It is seen that the theoretical analysis correctly predicts the general horizontal banded shape of the domain and that the low-gain boundary of the domain is in good quantitative agreement with the experimental observations. However, in contrast with the observations, the theoretical analy-

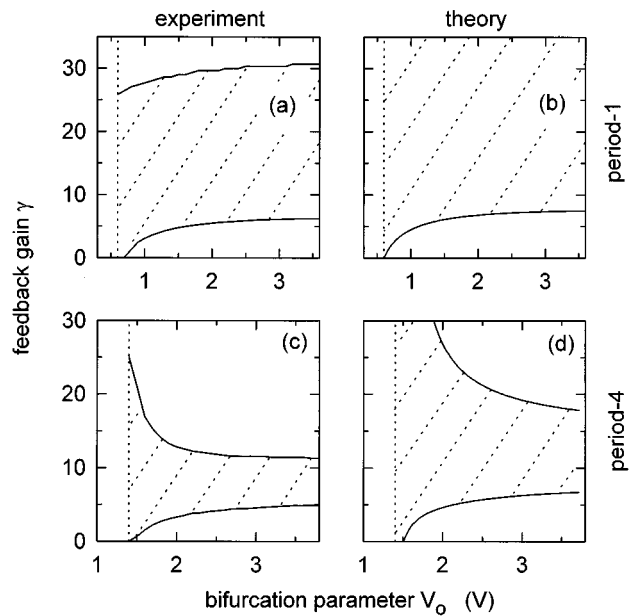


FIG. 16. Comparison of experimental and theoretical domains of control. We compare period-1 domains (a) and (b) at $R=0.68$, and period-4 domains (c) and (d) at $R=0.65$. The vertical dashed line marks the point at which the orbit becomes unstable in the absence of feedback. Note that the theoretically predicted domains assume $t_\ell=0$.

sis predicts that values of the feedback parameter γ larger than 1000 will give rise to successful control. Somewhat closer agreement between the observed and predicted domain of control is obtained for the period-4 orbit ($R=0.65$) as shown in Figs. 16(c) and (d), respectively. Similar results are obtained for other values of the control parameter R .

We find that the discrepancy between the theoretically predicted and experimentally observed domains of control is due primarily to the control-loop latency ($t_\ell=10$ ns for our implementation of ETDAS). To investigate the effects of t_ℓ , we turn to direct numerical integration of the time-delay differential Eqs. (2) and (A4). The equations are integrated using a fourth-order Adams-Bashforth-Moulton predictor-corrector scheme with a step size of 0.1 ns. Successful control is indicated when the ETDAS error signal falls to the machine precision in a time equal to 20,000 orbital periods. We note that this procedure may underestimate the size of the domain of control when the convergence is slow. To set the initial conditions for the time-delay differential equations, we integrate the equations without the time-delay terms (equivalent to the diode resonator in the absence of control), initially using a fourth-order Runge-Kutta algorithm. We store variable values, derivatives, and calculated time-delay in arrays as we integrate; these values are needed for the predictor-corrector routine and to determine $V_{\delta p}(t)$. We switch to the predictor-corrector integrator after ten cycles of Runge-Kutta and add the control terms. We note that despite the infinite series in Eq. (2), it is not required to retain all past variable values to calculate $V_{\delta p}(t)$; ETDAS can be expressed recursively, requiring only storage of the information from one past orbital cycle.⁸

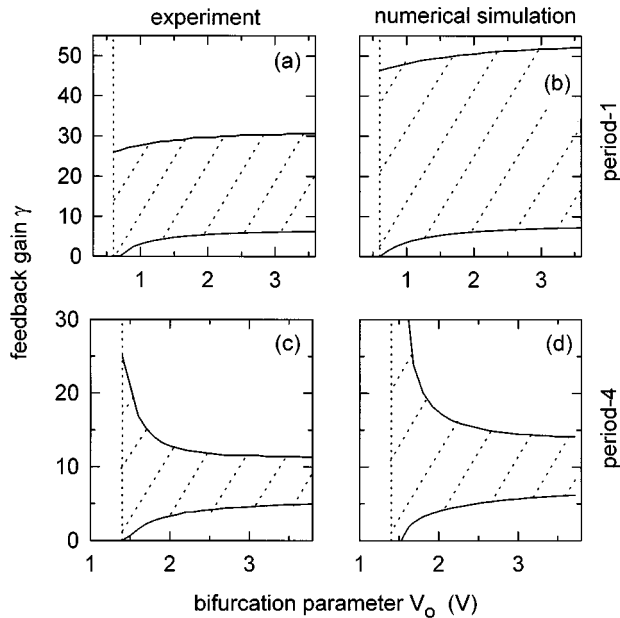


FIG. 17. Comparison of experimental and numerically simulated domains of control. The numerical simulations include a control-loop latency $t_\ell = 10$ ns. As in Fig. 16, we compare period-1 domains (a) and (b) at $R = 0.68$, and period-4 domains (c) and (d) at $R = 0.65$. The vertical lines again mark the point at which the orbits become unstable in the absence of feedback. Note that inclusion of control-loop latency improves the quantitative agreement of the results.

Figure 17 shows the experimental [period-1, Fig. 17(a); period-4, Fig. 17(c)] and numerically predicted [period-1, Fig. 17(b); period-4, Fig. 17(d)] domains of control for the UPOs with $t_\ell = 10$ ns and $R = 0.68$ (period-1) and $R = 0.65$ (period-4). It is seen that the agreement is improved, highlighting the fact that small control-loop latencies (only 10% of the orbital period for the period-1 UPO) can shift the domain of control.

G. Effects of control-loop latency

To illustrate the deleterious effects of large control-loop latency, we add an additional delay to the feedback signal by inserting various lengths of coaxial cable (type RG-58/U) between the output of the ETDAS error generating circuitry and the signal conditioning device at the input to the diode resonator. In this case, $V_{\delta p}(t) = V_{\delta p}^{ideal}(t - t_\ell)$, where the time-lag t_ℓ includes the latency of the ETDAS circuitry (10 ns) as well as that incurred by the coaxial cable. By introducing the additional time-lag, we mimic the situation in which slower electronic components are used in the ETDAS circuitry.

Figure 18 shows the range of γ that gives rise to successful control of the period-1 UPO as a function of t_ℓ for $V_0 = 1.9$ V, and $R = 0$ [Fig. 18(a)] and $R = 0.68$ [Fig. 18(b)]. For both cases, it is seen that increasing t_ℓ causes the range of γ to decrease until control is unattainable when the time-lag is approximately one-half of τ (100 ns). Stabilization of the orbit is possible for larger values of t_ℓ as a new region of control appears, although with the opposite sign of the feed-

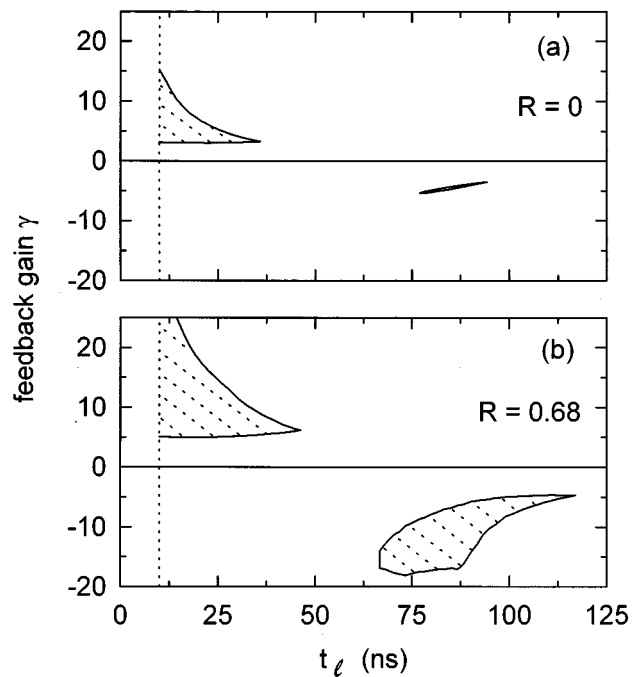


FIG. 18. Effects of control-loop latency t_ℓ on the domain of control for the period-1 UPO. Controlled regions are shown for $V_0 = 1.9$ V, (a) $R = 0$ and (b) $R = 0.68$. The dashed vertical line at $t_\ell = 10$ ns indicates the minimum latency attainable with our implementation of ETDAS.

back parameter γ . It is also seen that the range of γ that gives rise to control when $R = 0$ is much less than that when $R = 0.68$, indicating that ETDAS is more effective than TDAS in the presence of a time-lag. Control is not possible for $t_\ell > 120$ ns. For comparison, the correlation (memory) time of the system is approximately $\lambda^{-1} \approx 140$ ns, where λ is the largest conditional Lyapunov exponent characterizing the period-1 UPO in the absence of control. Hence, the correlation time appears to be the relevant parameter with regards to control-loop latency.

Similar results are obtained when stabilizing the period-4 orbit as shown in Fig. 19, although control fails for much smaller t_ℓ . It is seen in Fig. 19(a) that control is possible only to $t_\ell \approx 26$ ns for $R = 0$ and $t_\ell \approx 70$ ns for $R = 0.65$ in Fig. 19(b). The correlation time for the period-4 UPO is $\lambda^{-1} \approx 250$ ns. Also, the range of γ that gives rise to successful control is much larger for $R = 0.65$. The fact that ETDAS feedback extends significantly the range t_ℓ in comparison to that achievable by TDAS suggests that ETDAS may be effective in controlling the dynamics of systems that fluctuate on the nanosecond or even sub-nanosecond scale for which relatively small t_ℓ may be difficult to achieve.

In contrast to the behavior observed for the period-1 orbit, we find no islands of stability for $\gamma < 0$ at the longer time-lags. We do find, however, a small region where the orbit is stabilized intermittently around $t_\ell \approx 107 - 117$ ns when $R = 0.65$. The system alternates irregularly between intervals of 'noisy' period-4 behavior and intervals of chaotic behavior. The indicated region of Fig. 19(b) is the where the system resides near the period-4 orbit for at least 10% of the

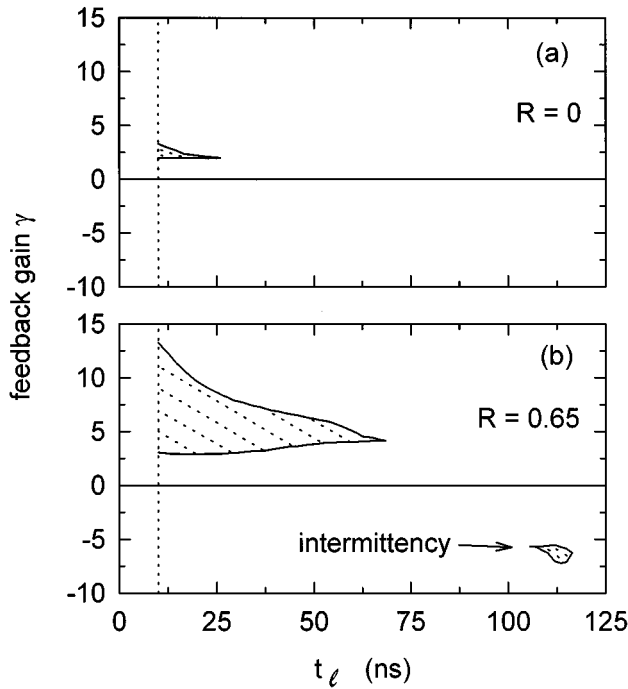


FIG. 19. Effects of control-loop latency t_ℓ on the domain of control for the period-4 UPO. Controlled regions are shown for $V_0=1.9$ V, (a) $R=0$ and (b) $R=0.65$. Note the region of intermittency for $\gamma < 0$ at large t_ℓ in (b). The dashed vertical line indicates the minimum latency of our circuitry.

time on average. Under some conditions, the systems remains near the UPO for ≈ 16 ms, corresponding to 40,000 orbital periods. Figure 20 shows examples of the dynamical evolution of the peaks V_n of $V(t)$ during this intermittent behavior. It is seen that the orbit can lose stability abruptly [Fig. 20(a)], or through a transition to other periodic behaviors [Fig. 20(b)]. We emphasize that these transitions do not result from a change in the feedback level, but occur spontaneously in the system.

H. Dynamics of the system outside the domain of control

We find it instructive to investigate the dynamics of the diode resonator in the presence of ETDAS feedback outside

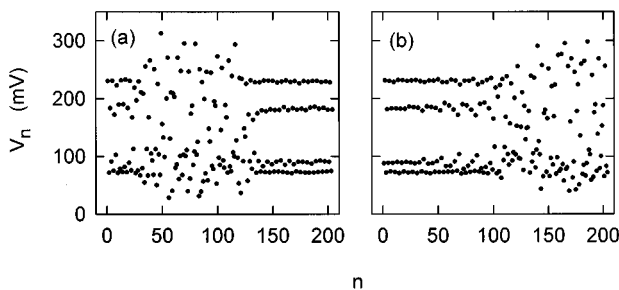


FIG. 20. Evolution of peak values V_n of $V(t)$ showing intermittent chaotic bursts away from period-4 UPO at $V_0=1.9$ V and $R=0.65$. (a) A short burst with $\gamma=7.4$ and $t_\ell=116$ ns. (b) Transition to a burst through periodic behavior with $\gamma=6.8$ and $t_\ell=112$ ns.

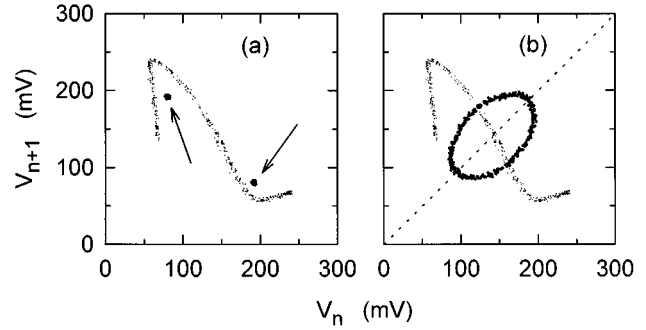


FIG. 21. First return maps illustrating the dynamics of the system outside of the domain of control. (a) The system displays period-2 behavior (shown by the two dark sets of points indicated by arrows) when the feedback gain is too weak ($\gamma=2.5$). These dots do not fall on the attractor of the unperturbed system (lighter dots), indicating the stabilized orbit is not a true UPO of the original system. (b) The system undergoes quasi-periodic dynamics (which appear as the dark oval centered on the period-1 fixed point) when γ is too large ($\gamma=17.5$). System parameters are $V_0=1.9$ V and $R=0$.

the domain of control to serve as a guide when attempting to control the dynamics of new systems. We explore the range of different behaviors by adjusting the feedback gain γ while fixing the other control parameters at $V_d=1.9$ V, $\tau=100$ ns (period-1 UPO control), $R=0$, and $t_\ell=10$ ns (its minimum value). For these parameters, the range of successful control of the period-1 orbit is approximately $3.14 < \gamma < 16.9$. Similar behaviors can be obtained by fixing γ and adjusting a different parameter or when attempting to control longer-period orbits.

As γ increases from zero to the lower boundary of the domain of control ($\gamma \sim 3.14$), the system goes from the chaotic state to the desired period-1 UPO through an inverse period-doubling cascade. Figure 21(a) compares the return map of the system without ETDAS feedback (light collection of points) and with feedback (dark collection of points indicated by arrows) for $\gamma=2.5$. It is seen that the system with feedback displays period-2 behavior that is not part of the original chaotic attractor since the points do not fall on the chaotic return map. The error signal $V_{\delta p}(t)$ is large in this case.

We find that the system displays quasi-periodic behavior when the feedback gain is larger than the higher boundary of the domain of control ($\gamma \sim 16.9$). Figure 21(b) shows the return maps of the system with and without feedback for $\gamma=17.5$ where it is seen that the points fall on an oval centered on the location of the period-1 fixed point. The temporal evolution of $V(t)$ displays oscillations around 10.1 MHz whose amplitude is modulated by low-frequency (~ 2 MHz) oscillations. For large values of γ , the low-frequency oscillations become more pronounced and the oval-shaped return map increases in size.

A more sensitive technique for investigating the dynamics close to the boundary of the domain of control is to perform a spectral analysis of $V(t)$. Figure 22(a) shows the spectrum of the signal $V(f)$ for $\gamma=3.1$, just outside the lower boundary of the domain of control. Clearly evident are spectral features at multiples of 5 MHz (the subharmonic of

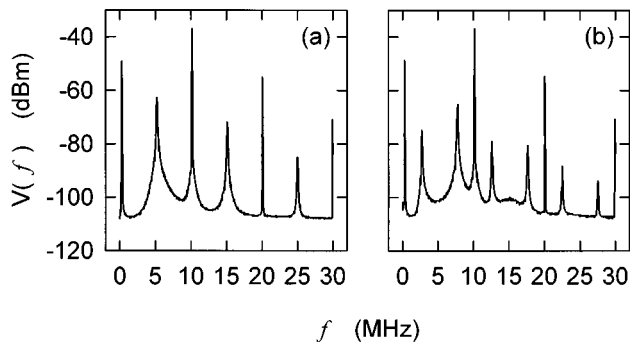


FIG. 22. Power spectra of $V(t)$ outside the domain of control for the period-1 UPO. (a) The spectrum has features at multiples of 5 MHz, indicating period-2 dynamics when the feedback gain is too weak ($\gamma=3.1$). (b) The spectrum displays sidebands displaced by 2 MHz, indicating low-frequency modulation of the fundamental frequency when the feedback gain is too strong ($\gamma=17.2$). System parameters are $V_0=1.9$ V and $R=0$.

the fundamental frequency) indicating period-2 behavior. Note that subharmonic peaks are >30 dB below the peaks of the fundamental frequency. Figure 22(b) shows the spectrum for $\gamma=17.2$, just above the upper boundary of the domain of control. Sidebands about the fundamental spectral features displaced by ~ 2 MHz appear in the spectrum, indicating the low-frequency modulation of the fundamental frequency. Note that these frequencies appear where the ETDAS feedback is less sensitive (recall the form of the transmission function of the ETDAS circuitry shown in Fig. 3). Hence, increasing R tends to suppress the growth of these frequency and enlarge the domain of control.

VI. CONCLUSIONS

Continuous feedback is a technique well-suited to controlling fast systems. Rather than generating a feedback that attempts to synchronize the system to an ideal reference state, we use in this experiment the ETDAS technique that continuously synchronizes the system to many cycles of its own past behavior. We stabilize period-1 and period-4 orbits of a diode resonator driven at 10.1 MHz, and demonstrate that the feedback signal becomes on the order of the noise level in the system when control is successful.

We show that control of the system is possible in previously uncontrollable areas of parameter space by increasing the parameter R , which corresponds to using more information from further in the past. Increasing R also broadens the range of feedback gains that effect control for a given drive strength. We also consider the time-lag t_ℓ on the effectiveness of the control, and demonstrate that control is possible at large time lags, particularly for larger values of R .

Given the optical analog of ETDAS, the next step in this work may be control in fast optical systems. A Fabry-Perot cavity may be able to stabilize the GHz frequency instabilities in semiconductor lasers subjected to weak stray reflections.^{8,34,35,37} Also, a version of ETDAS may be useful for controlling unstable steady states in dynamical systems if

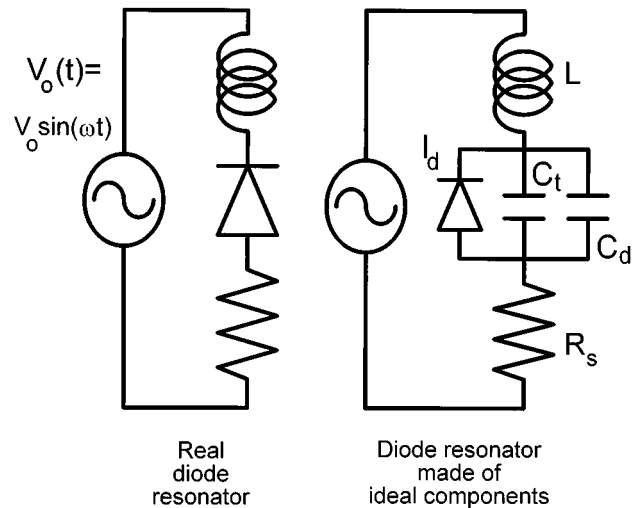


FIG. 23. Real and idealized diode resonator. The rectifier diode is considered to be made up of an ideal diode (described by the Shockley formula) in parallel with two voltage-dependent capacitances.

the fundamental frequency selected by the feedback is significantly greater than the fluctuations present in the system.⁵⁶

ACKNOWLEDGMENTS

DWS and DJG gratefully acknowledge financial support from the U.S. Air Force Phillips Laboratory under Contract No. F29601-95-K-0058, the U.S. Army Research Office under Grant No. DAAH04-95-1-0529, and the National Science Foundation under Grant No. PHY-9357234. MEB and JEES gratefully acknowledge financial support from the National Science Foundation under Grant No. DMR-94-12416.

APPENDIX A: A MODEL OF THE DIODE RESONATOR

To compare our experimental findings with theory, we describe the dynamics of the diode resonator by a set of coupled nonlinear differential equations delineated by Newell *et al.*⁵⁷ This model is well suited for rectifier diodes, such as the type 1N4007 in our resonator. Other types of diodes are more accurately described by different models.⁵⁰⁻⁵³

The model treats the real circuit as a collection of ideal components as shown schematically in Fig. 23. The resistor R_s and the inductor L accounts for the total reactance and inductance of the circuit, respectively. The rectifier diode consists of the parallel combination of: An ideal diode whose voltage-to-current characteristics is described by the Shockley formula

$$I_d = I_s [\exp(eV_d/\alpha k_B T) - 1], \quad (\text{A1})$$

where V_d is the voltage drop across the diode, I_s is the reverse-bias current, $e/k_B T$ is the thermal voltage, and α accounts for carrier recombination in the depletion zone; a voltage-dependent capacitor C_t accounting for the junction capacitance whose form is given by

$$C_t = \begin{cases} C_b(1 - V_d/V_J)^{-\beta} & V_d < V_J/2 \\ C_b(b_1 + \beta V_d/V_J)/b_2 & V_d \geq V_J/2 \end{cases}, \quad (\text{A2})$$

where C_b is the zero-bias junction capacitance, $V_J = 0.6$ V is the junction potential, β quantifies the variation of the doping concentration across the junction, and $b_1 = (1 - \beta)/2$ and $b_2 = 2^{-(\beta+1)}$ ensures that C_t is continuous; and a voltage-dependent capacitor C_d accounting for the diffusion capacitance, arising from the finite response time of carriers to a changing field, whose form is given by

$$C_d = C_0 \exp(eV_d/\alpha k_B T), \quad (\text{A3})$$

where C_0 is the zero-bias diffusion capacitance.

Using standard circuit analysis, the differential equations describing the diode resonator are given by

$$\frac{dV_d}{dt} = (I - I_d)/(C_d + C_t), \quad (\text{A4})$$

$$\frac{dI}{dt} = [-V_d - IR_s + V_0(t)]/L,$$

where I is the current flowing through the diode resonator, $V_0(t) = V_0 \sin \omega t$ with $\omega = 2\pi(10.1 \times 10^7)$ 1/s under normal operating conditions, and $L = 25 \mu\text{H}$ is the measured low-frequency inductance of the inductor.

We determine the values of the parameters by measuring several of the circuit characteristics. The parameters of the ideal diode are found by measuring the current flowing through the real diode (we remove it from the diode resonator for this measurement) as a function of an applied dc voltage. Reasonable agreement between the measured and predicted behavior is found with $I_s = 8.8$ nA and $\alpha = 1.79$. The ac characteristics of the diode resonator are determined by measuring its response to a weak sinusoidal modulation with a dc offset. Specifically, we measure $I(t)$ when the resonator is driven by a voltage $V_0(t) = V_{dc} + \delta V \sin \omega t$ as a function of ω for $-4 \text{ V} \leq V_{dc} \leq 0.5 \text{ V}$ and $\delta V \approx 890 \mu\text{V}$. The frequency response of the resonator displays a resonance due to the combined action of the inductor, capacitors, and resistors. The remaining circuit parameters are determined by fitting the predicted form of the resonance curve [Eq. (A4)] to the observed behavior. We find that the parameters change somewhat over the range of V_{dc} which may be a result of saturation of the inductor as the higher currents, an effect not accounted for in our model. The best overall fit yields $R_s = 245 \Omega$, $\beta = 0.33$, $C_0 = 0.2$ pF, and $C_b = 17$ pF.

¹F. J. Romeiras, C. Grebogi, E. Ott, and W. P. Dayawansa, *Physica D* **58**, 165 (1992).

²E. Ott and M. Spano, *Phys. Today* **48**, 34 (1995).

³In the nomenclature of modern control engineering, a control protocol that stabilizes a system about a state that is inherently part of the system is called a regulator control scheme.

⁴A system ergodically explores the neighborhoods of the infinite number of unstable states when it is chaotic. Targeting techniques can be used to direct the system to the desired state.

⁵K. Petermann, *IEEE J. Sel. Top. Quantum Electron.* **1**, 480 (1995), and references therein.

⁶G. H. M. van Tartwijk, A. M. Levine, and D. Lenstra, *IEEE J. Sel. Top. Quantum Electron.* **1**, 466 (1995), and references therein.

⁷Y. Liu, N. Kikuchi, and J. Ohtsubo, *Phys. Rev. E* **51**, 2697 (1995), and references therein.

⁸J. E. S. Socolar, D. W. Sukow, and D. J. Gauthier, *Phys. Rev. E* **50**, 3245 (1994).

⁹K. Pyragas, *Phys. Lett. A* **170**, 421 (1992).

¹⁰M. E. Bleich and J. E. S. Socolar, *Phys. Lett. A* **210**, 87 (1996).

¹¹M. Ciofini, R. Meucci, and F. T. Arecchi, *Phys. Rev. E* **52**, 94 (1995), and references therein.

¹²R. Mettin and T. Kurz, *Phys. Lett. A* **206**, 331 (1995), and references therein.

¹³R. Mettin, A. Hübler, and A. Scheeline, *Phys. Rev. E* **51**, 4065 (1995).

¹⁴E. Ott, C. Grebogi, and J. A. Yorke, *Phys. Rev. Lett.* **64**, 1196 (1990).

¹⁵Typically, Modern Control Engineers use a different, but equivalent, method for expressing the perturbations. For example, it is common to find the perturbations expressed as $\delta p_i = p_i - \bar{p} = -\mathbf{K}^T[\mathbf{z}_i - \mathbf{z}_*(\bar{p})]$ where \mathbf{K}^T is a $1 \times m$ feedback matrix (Ref. 16).

¹⁶K. Ogata, *Modern Control Engineering*, 2nd Ed. (Prentice-Hall, Englewood Cliffs, NJ, 1990).

¹⁷W. L. Ditto, S. N. Rauseo, and M. L. Spano, *Phys. Rev. Lett.* **65**, 3211 (1990).

¹⁸E. R. Hunt, *Phys. Rev. Lett.* **67**, 1953 (1991).

¹⁹B. Peng, V. Petrov, and K. Showalter, *J. Phys. C* **95**, 4957 (1991).

²⁰T. W. Carr and I. B. Schwartz, *Phys. Rev. E* **50**, 3410 (1995).

²¹T. W. Carr and I. B. Schwartz, *Phys. Rev. E* **51**, 5109 (1995).

²²Z. Qu, G. Hu, and B. Ma, *Phys. Lett. A* **178**, 265 (1993).

²³S. Bielański, M. Bouazaoui, D. Derozier, and P. Glorieux, *Phys. Rev. A* **47**, 3276 (1993).

²⁴G. A. Johnson and E. R. Hunt, *IEEE Trans. Circuits Syst.* **40**, 833 (1993).

²⁵K. Pyragas and T. Tamaševičius, *Phys. Lett. A* **180**, 99 (1993).

²⁶D. J. Gauthier, D. W. Sukow, H. M. Concannon, and J. E. S. Socolar, *Phys. Rev. E* **50**, 2343 (1994).

²⁷A. Namajūnas, K. Pyragas, A. Tamaševičius, *Phys. Lett. A* **204**, 255 (1995).

²⁸S. Bielański, D. Derozier, and P. Glorieux, *Phys. Rev. E* **49**, R971 (1994).

²⁹Th. Pierre, G. Bonhomme, and A. Atipo, *Phys. Rev. Lett.* **76**, 2290 (1996).

³⁰T. Hikiyama and T. Kawagoshi, *Phys. Lett. A* **211**, 29 (1996).

³¹M. Ye, D. W. Peterman, and P. E. Wigen, *Phys. Lett. A* **203**, 23 (1995).

³²E. Schöll and K. Pyragas, *Europhys. Lett.* **24**, 159 (1993).

³³C. Lourenço and A. Babloyantz, *Neural Comput.* **6**, 1141 (1994).

³⁴W. Lu and R. G. Harrison, *Opt. Commun.* **109**, 457 (1994).

³⁵C. Simmendinger and O. Hess, *Phys. Lett. A* **216**, 97 (1996).

³⁶R. Martin, A. J. Scroggie, G.-L. Oppo, and W. J. Firth, *Phys. Rev. Lett.* **77**, 4007 (1996).

³⁷K. Pyragas, *Phys. Lett. A* **206**, 323 (1995).

³⁸A map-based version of ETDAS was proposed independently by E. H. Abed, H. O. Wang, and R. C. Chen, *Physica D* **70**, 154 (1994).

³⁹W. Just, T. Bernard, M. Ostheimer, E. Reibold, and H. Benner, *Phys. Rev. Lett.* **78**, 203 (1997).

⁴⁰M. E. Bleich, D. Hochheiser, J. V. Moloney, and J. E. S. Socolar, *Phys. Rev. E* **55**, 2119 (1997).

⁴¹M. Born and E. Wolf, *Principles of Optics*, 6th ed. (Pergamon, New York, 1980), Sec. 7.6.1.

⁴²Analog Devices, One Technology Way, P.O. Box 9106, Norwood, Massachusetts 02062-9106.

⁴³Press-n-Peel film #100PNPR, Techniks, Inc., P.O. Box 463, Ringoes, New Jersey 08551.

⁴⁴Andrew Corporation, 10500 W. 153rd Street, Orland Park, Illinois 60462.

⁴⁵Hewlett-Packard, 3000 Hanover Street, Palo Alto, California 94304-1185.

⁴⁶Kay Elemetrics Corp., 12 Maple Avenue, P.O. Box 2025, Pine Brook, New Jersey 07058-2025.

⁴⁷J. Perez and C. Jeffries, *Phys. Lett. A* **92**, 82 (1982).

⁴⁸C. Jeffries and C. Perez, *Phys. Rev. A* **26**, 2117 (1982).

⁴⁹R. Hilborn, *Phys. Rev. A* **31**, 378 (1985).

⁵⁰P. S. Linsay, *Phys. Rev. Lett.* **47**, 1349 (1981).

⁵¹J. Testa, J. Perez, and C. Jeffries, *Phys. Rev. Lett.* **48**, 714 (1982).

⁵²R. W. Rollins and E. R. Hunt, *Phys. Rev. Lett.* **49**, 1295 (1982).

⁵³E. R. Hunt and R. W. Rollins, *Phys. Rev. A* **29**, 1000 (1984).

⁵⁴Z. Su, R. W. Rollins, and E. R. Hunt, *Phys. Rev. A* **40**, 2698 (1989).

⁵⁵Tektronix, Inc., 26600 SW Parkway, P.O. Box 1000, Wilsonville, Oregon 97070-1000.

⁵⁶A. Chang, G. M. Hall, J. R. Gardner, and D. J. Gauthier (preprint).

⁵⁷T. C. Newell, P. M. Alsing, A. Gavrielides, and V. Kovanis, *Phys. Rev. E* **51**, 2963 (1995).